# SUPERSONIC SEPARATION WITH OBSTRUCTIONS

By

SHASHI BHUSHAN VERMA

DEPARTMENT OF AEROSPACE ENGINEERING

INDIAN INSTITUTE OF TECHNOLOGY KANPUR

MAY, 1993

SUPERSONIC SEPARATION WITH OBSTRUCTIONS

by

Shashi Bhushan Verma

thesis submitted in partial fulfillment of
Master of Technology

to

Department of Aerospace Engineering
Indian Institute of Technology
Kanpur - 208 016, India

AE-1993-M-VER-SUP+

DEDICATED TO

THE

ALMIGHTY

7/5/93

CERTIFICATE

This to certify that this work entitled, "SUPERSONIC
SEPARATION WITH OBSTRUCTIONS" has been carried out by
Shashi Bhushan Verma under my supervision and that
this has not been submitted elsewhere for a degree.

(Dr. Vijay Gupta)
Professor
Department of Aerospace Engineering
Indian Institute of Technology
Kanpur - 208 016, India

7 May, 1993

ACKNOWLEDGMENTS

CONTENTS

ABSTRACT

An experimental investigation has been carried out to study supersonic separation caused by obstacles placed in boundary-layer flows. Particular emphasis is paid to the details of the flow near the leading edge of the obstacles. An effort has been made to gain insight of the flow structure in its vicinity.

The study relies on the flow patterns as revealed by flow visualisation supplemented by Schelieren studies wherever required and pressure studies along the medial line ahead of the obstacle.

Data has been obtained for blunt obstacles of varying heights, diameter and geometry and at various boundary-layer thicknesses. Correlations have been developed which best fit the data obtained for the range and conditions under which the tests have been carried out.

C H A P T E R   1

Introduction

The complex problem of the supersonic flow along a flat plate as it interacts with blunt obstructions has received considerable attention in recent past. The presence of the blunt obstruction in supersonic flow causes the formation of bow shock wave ahead of the obstruction. The adverse pressure gradient resulting from the bow shock wave propagates upstream in the subsonic flow within the boundary layer and results in the separation of the boundary layer and formation of vortices ahead of the obstruction. These vortices scavenge the boundary layers leading to increased pressure and heat transfer loads. A similar phenomena ahead of partially closed inlets is responsible for the buzz phenomena associated with supersonic inlets. As a matter of fact, it is this problem which provided the immediate motivation to undertake this study to understand some aspects of the boundary layer interactions with three-dimensional protuberances on flat plates in supersonic flows.

In a survey of the effects of protuberances in the boundary layer flows, Sedney and Kitchens[1] classify protuberances as small or large depending upon the disturbance they produce in the boundary layer. They showed that such protuberances whose dimension normal to the plate is less than

the boundary layer thickness so that they are completely buried within the boundary layer maybe classified as small protuberances. The other dimensions are not restricted. Fig 1.1 shows the geometry of a two dimensional step as opposed to a three dimensional protuberance.
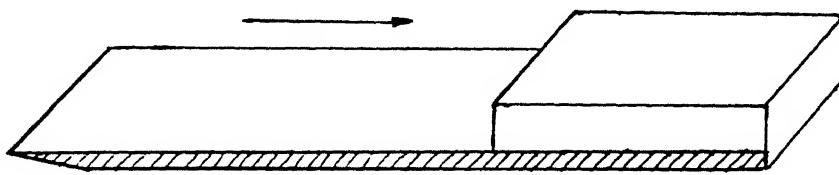
2 D   STEP
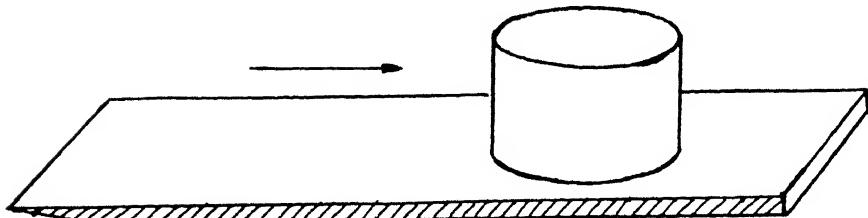
3 D   STEP

Fig 1.1 Geometry of 2-D step as opposed to 3-D obstacle

The separation phenomena associated with two dimensional steps and the resultant planer shocks have been well studied as far back as early 1950's. A theoretical formulation involving turbulent boundary layers has been reported by Mager[2-3]. The pressure rise at the two dimensional step face established an oblique shock wave that propagated upstream and caused the

boundary layer to separate from the base plate. Fig 1.2 shows the postulation of the separation caused by a two-dimensional step as determined by R.Lange[4] from shadowgraphs.

MAIN SHOCK
M
SHOCK
MIXING ZONE
δ
STEP   H
DIRECTION OF
CIRCULATION
SEPARATED
REGION
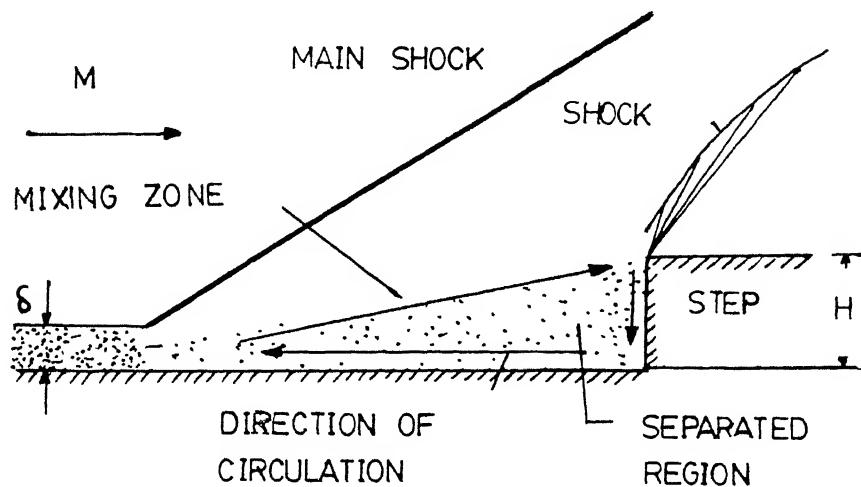
Fig 1.2 Separation caused by 2-D step as postulated by Lange

Here the main oblique shock causes the boundary layer to separate. The high speed mixing zone produced behind the oblique shock impinges on the step to cause a bow shock wave to appear immediately ahead of the step. The length of the high pressure region down-stream of the shock wave upto the leading edge of the obstruction was found to be a function of the step-height to boundary-layer thickness ratio whereas the "plateau" pressure reached in this region was found to depend on the upstream Mach number. This was confirmed in a number of

experimental studies(Chapman el.at[5] and Halprin[6]). See Fig 1.3

The phenomena is far more complex with three-dimensional
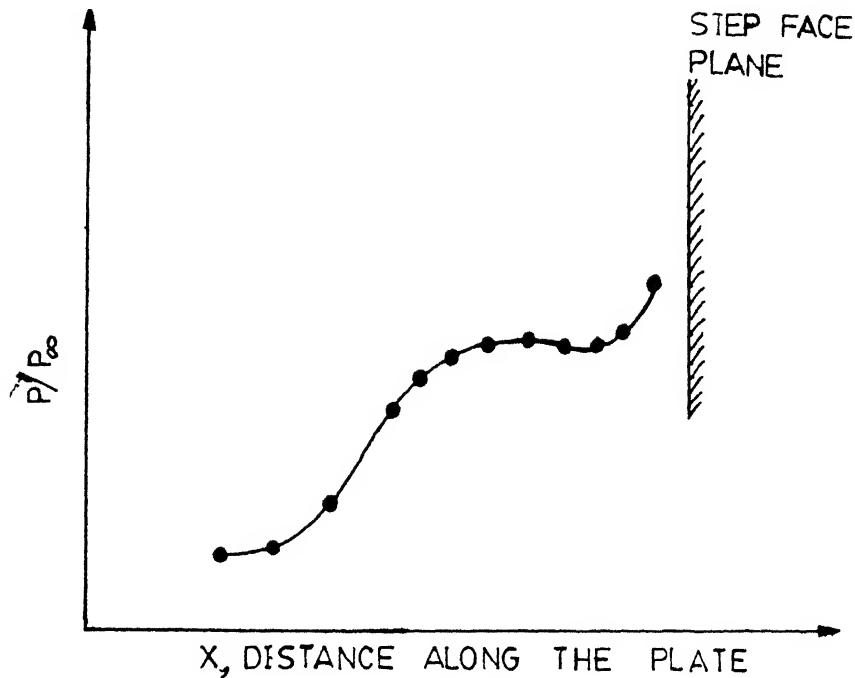
Fig 1.3 Pressure distribution ahead of a 2-D step.

obstructions. The complexities arise from the circumferential flow and the associated lateral pressure relief afforded by the limited lateral dimensions as opposed to the two-dimensional steps. The nature of separation depends upon the type of upstream flow,i.e, if it is laminar or turbulent and on the Mach number of the flow. The shape of the protuberance and its vertical dimension also play a leading role.

Analytic formulations of this problem are essentially very rudimentary and experimental investigations are almost

mandatory. Flow visualization offers valuable insights into the associated complex flow phenomena. Most of the flow visualization studies rely on surface flow patterns.

Surface flow patterns can be quite revealing and can indicate the lines of separation, lines of reattachment, streamwise vortices and appearance of turbulence. Various oil mixtures have been reported in literature. It has been mentioned that it is an art to obtain a mixture of correct consistency which will flow in the regions close to separation lines where shear stress levels are low and still will not be blown asunder in the tunnel starting and stopping processes. Westkaemper[7] reports using a blue dye dissolved in naptha and injected through holes upstream of test stations.

One disadvantage of using surface flow technique is that it affords very little information about the location of shocks and hence the shock-boundary layer interaction. Sedney and Kitchens[1] report a very ingenuous optical surface indicator technique. In this the obstacle is mounted on a test section window using a bolt and a seal as shown in Fig 1.4 .

A small amount of lightweight transparent oil is placed on the window before the flow is started. After the flow pattern is established, a shadowgraph or a Schlieren picture is taken. These plan- view pictures show the surface flow patterns and the parts of the shock surfaces.

Halprin[6] on the basis of extensive flow visualization and

LIGHT RAYS

M>1

SHOCKS

δ

OIL DOTS

H

WINDOW

FILM
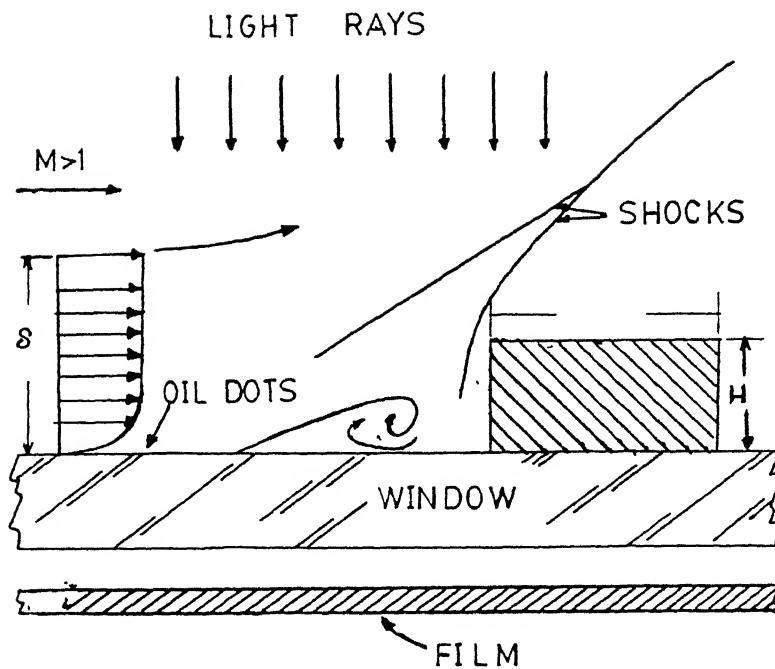
Fig 1.4 Optical surface-indicater technique

surface pressure studies postulates that the boundary layer

that separates from the plate and becomes a viscous shear layer

is forced over the two dimensional step so that only the low

energy separated flow impinges on the step face as shown in Fig

1.5. But the pressure relief offered by the circumferential

flow in three dimensional obstacles allows the compression

region to shrink in size and permits the high speed viscous

shear layer to impinge on the step face. This establishes a
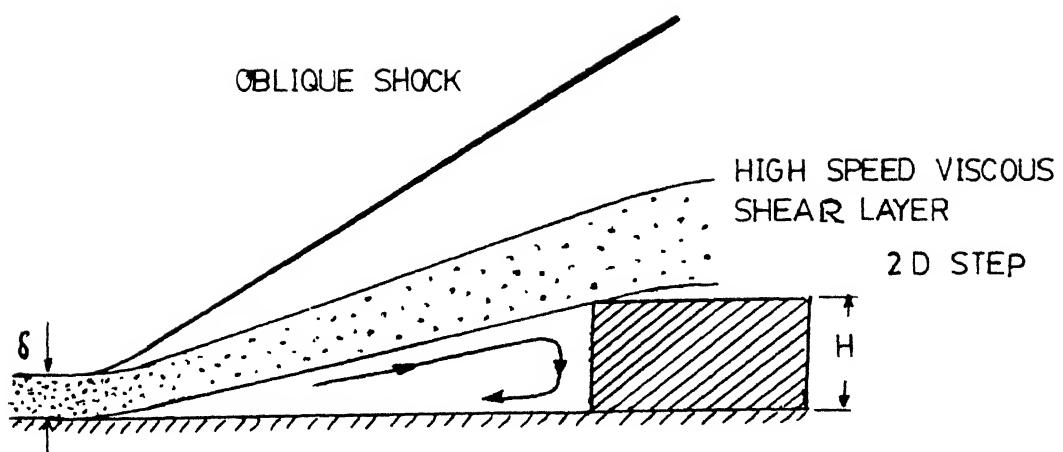
Fig 1.5 Nature of separation ahead of a 2-D step

second shock(Fig 1.6,Sykes[8]) and changes the pressure pattern on the static plate as shown in Fig 1.7(Halprin[6]).

Based on these studies , Halprin[6] proposed a three region model(Fig 1.8)for the plate region from the primary separation to the face of the obstacle. The outermost region is located immediately behind the oblique shock wave that is formed upstream of the step and consists of the flow which is directed circumferentially around the obstacle. It is in this region that the plate pressure builds up to a first maxima. The second region, inside the first, is characterized by radial flow
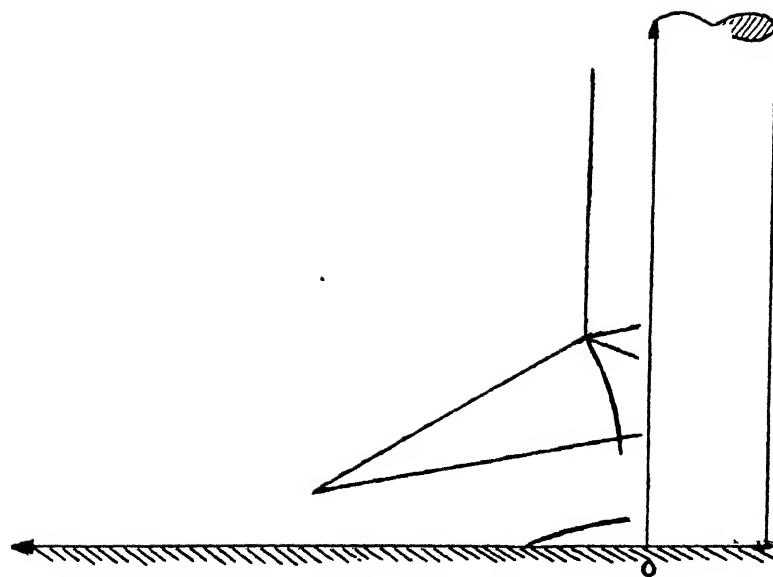
Fig 1.6 Shock stucture ahead of a 3-D obstacle.
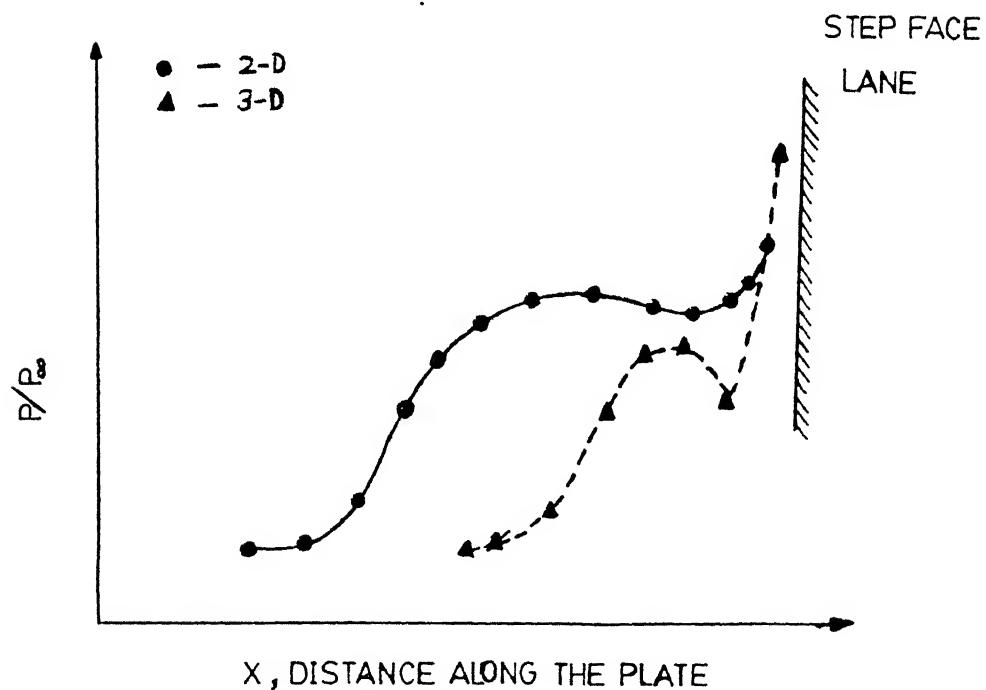
Fig 1.7 Pressure pattern for a 3-D obstacle as opposed to a

2-D step

OBLIQUE SHOCK

BOW SHOCK

VISCOUS SHEAR LAYER

BOUNDARY LAYER

CYLINDRICAL STEP

STAGNATION REGION
RADIAL FLOW REGION
CIRCUMFERENTIAL FLOW REGION
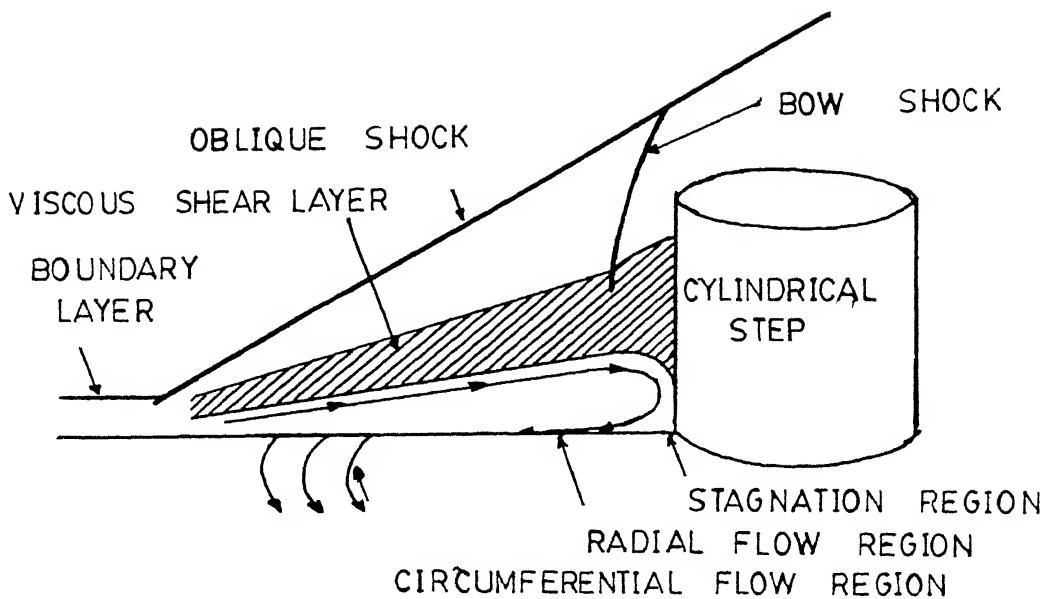
Fig 1.8 Three-region model proposed by Halprin.

directed away from the step along the plate. This flow is the
result of a horseshoe vortical flow established around the
obstacle, and a sizable dip in the pressure should be observed
in this case. A third region exists close to the obstacle in
which a low speed high pressure flow is apparent.

This model is supported by the results of measurements of
pressure along the length of the cylinder supported at one end
on a plate, Fig 1.9 (Westkaemper[9]). Figure shows the pressure
coefficient along the stagnation line of the cylinder.

It may be seen that the minimum pressure point on the
cylinder does not occur at the cylinder plate junction, but
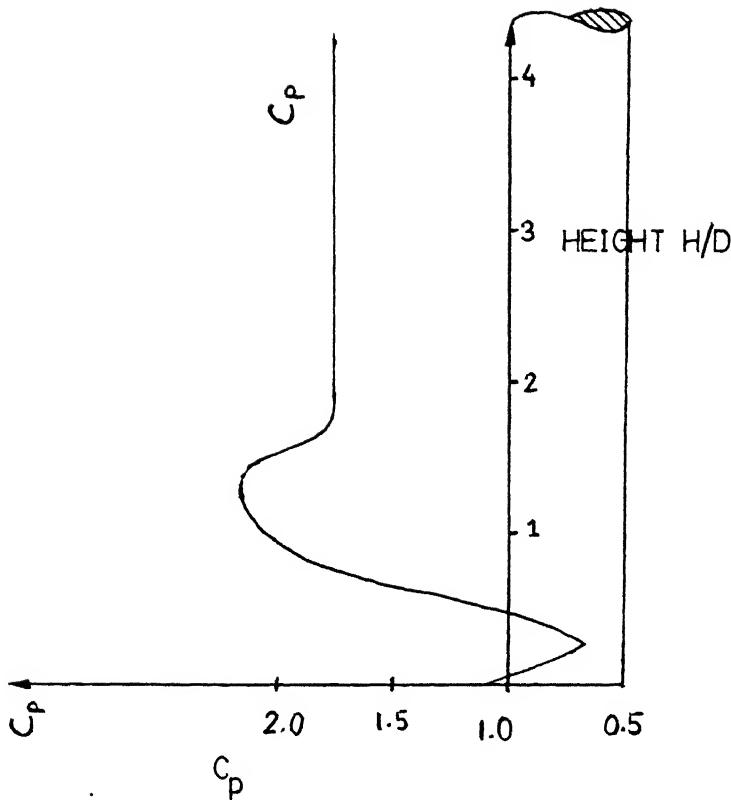
Fig 1.9 Pressure coefficient along the stagnation line of the
cylinder

rather at a small distance out along the cylinder. The minimum
coincides approximately with the lower edge of the separated
boundary layer. This suggests the Halprin's[6] hypothesis of a
third region of low energy flow below the separated boundary
layer. Rise in pressure at the plate cylinder junction
similarly agrees with the suggestion that the junction is a
stagnation point.

Korkegi[10] reports that the pressure distributions along the
leading edge of the fins or cylinders reflect a rise above the
stagnation point values below the triple point of lambda shock
followed by a sharp drop off at the foot. This is

characteristic of higher pressure recovery following compression through oblique shocks. Westkaemper[8] utilizes a pressure rise relation to estimate the height of triple point(which is a characteristic of three-dimensional obstacles) and the peak pressure on the leading edge.

Westkaemper[9] investigated through Schlieren photography the effect of model size on the flow around the cylinder. He showed that for small heights the boundary layer does not separate. The influence of model diameter for cylinder of large height is marked. The large diameter cylinders have a larger compression region in line with the suggestion that it is the three-dimensionality which provides the pressure relief and hence controls the size of the compression region.

The surface flow patterns observed by various authors have resulted in the evolution of a rather complex model for the surface flow ahead of the obstacle.

The reverse flow initiated by the separated boundary layer marks the beginning of the formation of a large scale vortex system ahead of the cylinder. This vortex is washed down-stream and thus is wrapped around the cylinder giving rise to a horse-shoe vortex. The streamlines away from the medial stagnation plane of the cylinder are bent by the oncoming flow in their direction. After some point this flow restricts the oncoming reverse flow from further points on the cylinder. This reverse flow is then rolled up to form another vortex and hence

the secondary separation line comes into picture. See Fig 1.10 (from our data).
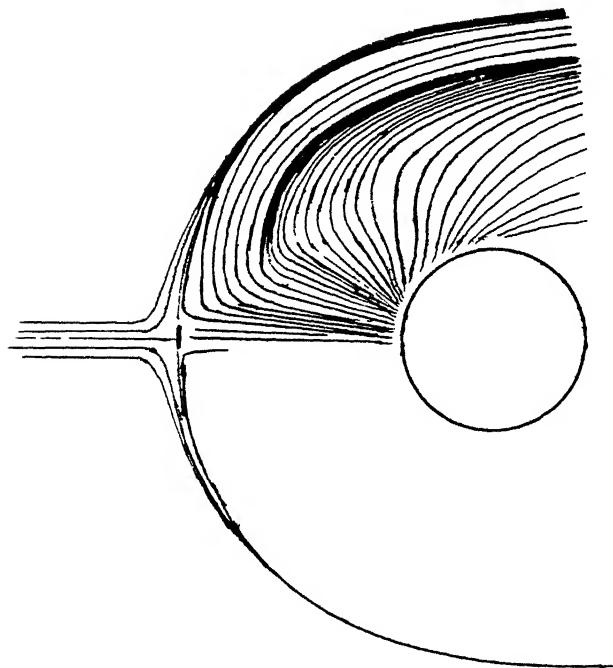
Fig 1.10 Streamline pattern developed from our test results.

Sedney[11] reports the presence of upto four horseshoe vortices rotating in alternate directions. The traces of these vortices are seen in the surface flow patterns as a series of separation lines behind the primary separation line.

Fig 1.11 (Korkegi[10]) shows a postulated vortical flow behind the primary separation line for a cylinder developed on the basis of oil flow photographs.
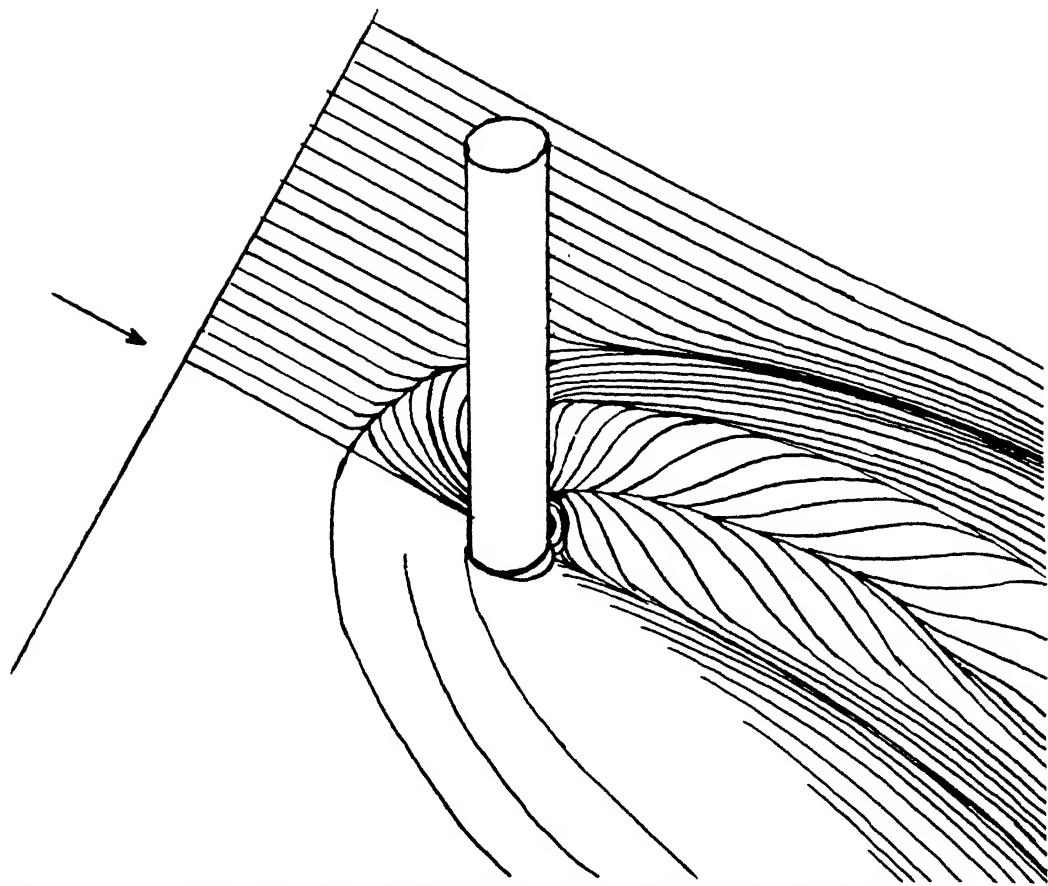
Fig 1.11 Vortical flow behind the primary separation line for a
cylinder as postulated by Korkegi.

A possible streamline pattern in the plane of symmetry of
the cylinder, which can possibly result in the observed pattern
of surface flow has been postulated by Ozcan and Holt[12](Fig
1.12). As reported by them, the number of separation lines
decreases from 3 to 2 to 1 as the Reynolds number(based on the
distance along the plate from its leading edge to the
cylindrical obstruction) of the flow was increased from 1.9 x
10^5 to 2.5 x 10^6.

In addition to the large scale vortices, evidence
indicates[11] a counter rotating small scale vortex located close
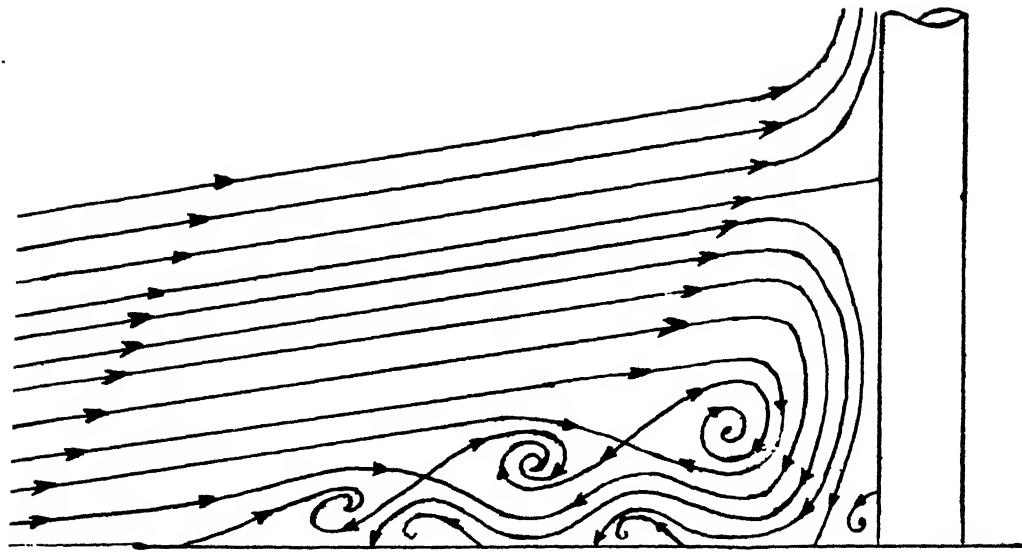
Fig 1.12 Streamline pattern in the plane of symmetry of the
cylinder as postulated by Ozcan and Holt.

to the base of the cylinder with scale size smaller than the
diameter. This small scale vortex also gets wrapped around the
cylinder and like other vortices trail downstream. This vortex
is indicated in oil flow patterns by an attachment line. This
attachment line is related to the region of maximum heating
rates on the surface. Burned marks have been observed by
Korkegi[10] near the base of fins that extend downstream at an
angle to the fin. These local high heating rates are associated
with the reattachment line. This region also being a region of
maximum shear rates is difficult to detect in visualization
studies. The reattachment lines have been observed for both

small and large values of H. Several vortices have been evident for large values of H/δ(where δ is the boundary layer thickness at the obstacle location), but only large scale and counter rotating vortices have been observed for H/δ = 1.

A number of investigators have attempted a correlation for the separation distance S, in the freestream direction, defined by Sedney and Kitchens[1] as the distance from the leading edge of the obstacle to the primary separation line. Holt[12],Korkegi[10],Halprin[6],R.Lange[4] have determined the separation distance by measuring the static pressure distribution along the medial line. In this technique the primary separation point is defined as the point where the surface pressure first deviates from the undisturbed upstream reading. Korkegi[10] and Sedney[11] have attempted to determine this distance by obtaining the heat transfer coefficient variation along the same line. Side view Schlieren or shadowgraph is another way of determining this distance(Westkaemper[9], Sedney and Kitchens[1]).

But the most popular method is the surface indicator technique. Settles et al[13] discuss that in both two-dimensional and three-dimensional flows the four techniques outlined above give different estimates of the separation distance. The surface flow visualization apparently gives the most reliable results which are repeatable. This mismatch in the separation distance values has been explained away as due to the

unsteadiness that exists in the flow field which thus hinders uniform experimental definition of separation for different techniques. Static pressure/heat transfer values have not been found to be repeatable due to the unsteady flow structures and have usually resulted in overprediction of S values. Extrapolation of shock wave through the boundary layer from Schlieren photographs also have resulted in unreliable results. Surface indicator technique with slow response time has been found to give an average flow pattern that is clear and repeatable[1].

Sedney and Kitchens[1] show that most important of the dimensionless parameters that have significant effect on S/D values are the ratio H/D and the Mach number M of the flow :

$$S/D = f(M, H/D)$$

where M is the freestream Mach number of flow,

H is the height of the obstacle in z-direction,

D is the diameter of the cylindrical obstacle

Though the dependence of S/D on M has been found to be weak in earlier studies(Westkaemper), it has been observed to increase with M. This is due to the variation in the value of δ with M.

A significant effect of H/D on S/D values has been

reported. It has been observed to increase with increase in H/D values until at some point where it approaches an " infinite effective height " case. At this point S/D assumes an almost constant value for further increases in H/D values. This provides an upper limit to S/D value. It has been observed that the rate of approach to this limit/asymptote depends upon D/δ. A large protuberance is thus defined by Sedney[5] on the basis of S/D ; that for which S/D differs by a small fraction from the asymptotic value. It has also been found that S/D is independent of D for large protuberances.

Various attempts have been made to correlate the separation distance ahead of the obstacle to the height of the obstacle. For smaller cylindrical obstacle, the data of Halprin[6] and of Westkaemper[4] suggest that the non-dimensional separation distance S/D varies with H/D as

$$S/D = 2.42 \ (\ H/D \ )^{0.7}$$

This variation appears to be valid for cylinders that have an H/D value greater than 0.1 or to those which extend out of or to the edge of the boundary layer, since very short protuberances will not cause separation. However a lower limit cannot be defined. For large H/D values, the correlation approaches to the " infinite length cylinder " case where S/D

assumes an almost constant value of 2.65 for H/D > 1.13. The correlation also indicates a weak dependence of M and Reynolds number on S/D values.

Korkegi[10] reports value of S/D ranging between 2-2.5 upstream of the fin leading edge. Sedney and Kitchens[1] observe from the data from other sources that for large obstacles, S/D does not depend on H/D. They also observe that variation of S with R_D(Reynolds number based on the diameter of the cylinder) is not very large for both small and large cylinders, but the complex structure within the separated pocket changes significantly. This change is noticed by change in number of vortices ahead of cylinder leading edge with R/X(units Reynolds number of the flow). This sensitivity is however not understood.

Thus for large obstacles,

$$S/D = f(M)$$

It has been observed by Ozcan and Holt from separation data(oil photographs) and static pressure measurements along the axis of symmetry that separation occurs in the increasing pressure region between the initial pressure rise and pressure plateau (P_p). Downstream of the plateau region, the pressure drops significantly, reaches a minimum valley pressure and increases through the detached bow shock. The secondary

separation occurs in the increasing pressure region for the reverse flow between the pressure valley and pressure plateau.

A comparison of streamwise and spanwise pressure distributions by them show that the location of initial pressure rise moves downstream with increasing Y/D (Y being the lateral dimension along the plate width). large streamwise and spanwise pressure gradients were observed within an approximately two dimensional vicinity of cylinder axis.

Ozcan and Holt[12] studied the flow in the vicinity of the obstacle using a laser velocimeter. It was observed that the magnitude of the reverse velocities and the height of the reverse flow region increases with decreasing -X/D. The magnitude of the maximum reverse velocity levels off for a particular -X/D range and the height of the reverse flow region decreases with further decrease in -X/D. From spanwise measurements, it was observed that the height of the reverse flow region and the magnitude of reverse velocities decrease with increasing Y/D.

He thus concludes that the velocity measurements show an unsteady flow structure and do not confirm the streamline pattern of Fig 1.12.

C H A P T E R   2

Scope of Present Study

An attempt has been made in the present experimental study to gain an understanding of the flow field in the vicinity of a three-dimensional protuberance as it interacts with a boundary layer in a supersonic stream. Particular emphasis is placed on the details of the flow near the leading edge of the obstacle.

The study relies on the flow patterns as revealed by surface-flow visualization supplemented by Schlieren studies wherever required or feasible and some pressure studies in the medial line ahead of the protuberance.

The principle objective of the study is to investigate the dependency of primary separation distance on

(a)   the variation of the lateral dimensions of the protuberance

(b)   the height of the protuberance as it relates to the thickness of the boundary layer at the location, and

(c)   geometry of the protuberance.

Model Design

The model used in the study consists of obstacles of various sizes and shapes mounted on a splitter plate which is

carefully aligned with the flow direction. The purpose of the splitter plate is to provide a leading edge from where the growth of the boundary layer starts, so that the thickness of the boundary layer along the plate varies with the distance and can be estimated.

The model used consists of an MS plate, ground flat, which is mounted in the test-section of the wind-tunnel such that it spans the width of the tunnel. The clearance between the plate edges and the side-walls was sealed using a shaped rubber gasket mounted flush with the surface.

The leading edge of the plate was made sharp so as to ensure supersonic flow on the plate. The shock wave from the leading edge was seen to be attached and weak enough to be neglected. Thus, the system produced a flow parallel to the plate at the designed Mach number.

The plate had a series of pressure taps along the medial line, each with a diameter of 0.5mm, carefully drilled and deburred. Each tap was connected through stainless steel tubes running along the bottom of the plate to a pressure multiplexer.

The model protuberances were mounted on the flat plate at two distances from the leading edge, representing two different boundary-layer thicknesses. Fig 2.1 shows an isometric view of the plate with dimensions, direction of chosen axis and the distances of the two locations on which the models were mounted

for the present study.

All the tests were conducted at a single Mach number   value
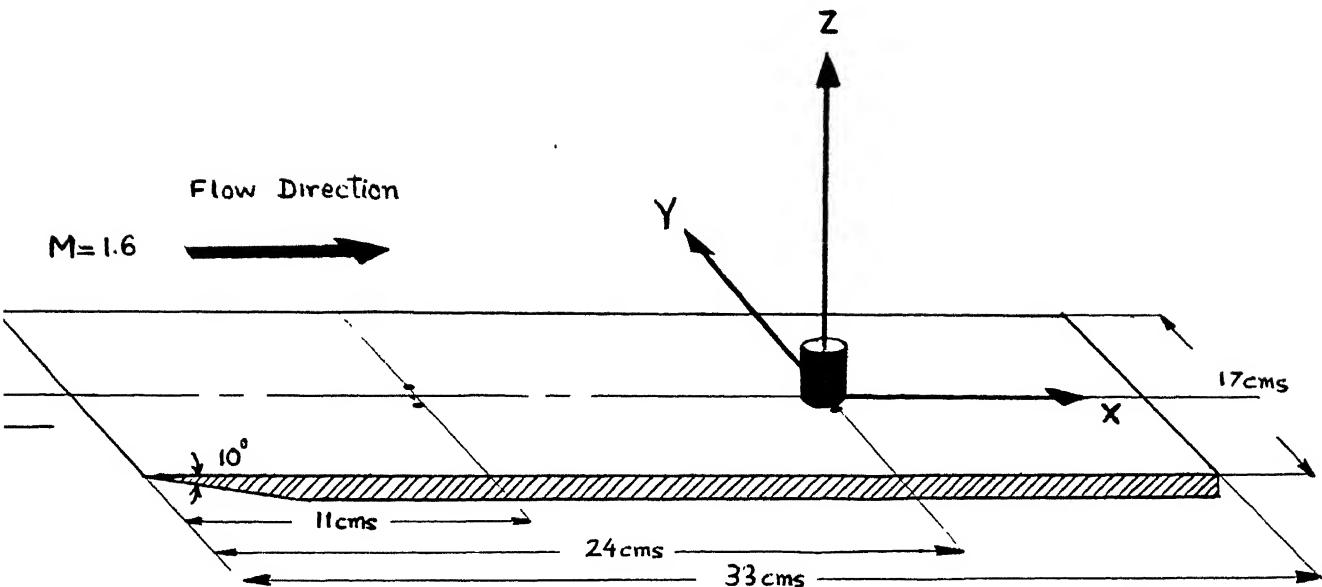
Fig 2.1   Isometric view of the plate model

of 1.60, and a constant stagnation pressure of 48.98 psia.   The
stagnation   temperatures   were fairly constant   for   all   flows
being between $13^{\circ}C$ and $14^{\circ}C$.

The unit Reynolds number is given by

$$Re = \frac{P_0 \sqrt{\gamma/R}}{\mu \sqrt{T_0}} \frac{M}{\left[1 + \frac{\gamma-1}{2} M^2\right]^{\frac{\gamma+1}{2(\gamma-1)}}}$$

where,

P_0 is the stagnation pressure of the flow

γ is the ratio of the specific heats

R is the gas constant

M   the Mach   number of the   flow

μ the viscosity of the air in the tunnel

T_0 the stagnation temperature of the flow

The given test conditions result in a unit Reynolds   number Re   of 3.61×10^7 m^{-1}. Thus the two test lengths L_1=24cms   and L_2=11cms   give $Re_L = 8.67 \times 10^6$ and $Re_L = 3.97 \times 10^6$ for   the boundary layer flows.

The   boundary layer thickness at the two locations   can   be estimated using the relation for incompressible flows,

$$\delta_i = 0.37x/(Re_x)^{1/5}$$

where,

x   is the distance from the leading edge   of
the plate to the location on it where the
model is mounted

Re_x the local Reynolds number on the plate

However,   for compressible flows Van Driest[14]   developed   a relation   and   plotted the values of the ratio δ_c/δ_i for   Mach numbers greater than unity. From that plot this ratio for M=1.6 turns out to be

$$\delta_c / \delta_1 = 1.02$$

Thus, in our case the boundary layer thickness for X1 =24cms and X2=11cms locations, keeping in view the above values turn out to be δ_{X1}=3.64 mm and δ_{X2}=2.0 mm.

Wind Tunnel

The wind tunnel which has been used for the purpose of present experimental investigation is an intermittent, blowdown type trisonic wind tunnel. A pair of two dimensional symmetric fixed nozzle block designed for a test-section Mach number of 1.6 and carved in wood was used.

Major specifications of the wind tunnel are listed in Table 2.1 .

Flow Visualization

The methods used for visualization of flow structure in the vicinity of the obstacle are the Schlieren and Surface flow technique.

For the purpose of shock pattern observation, the side walls of the tunnel test-section have been provided with two sets of 9 inch diameter Schlieren windows. The 9 inch Schlieren system uses two parabolic mirrors and an air-cooled mercury-

vapour lamp. A video recording and display system on TV screen

Table 2 1

MAJOR SPECIFICATIONS OF WIND TUNNEL

Test Section Size	0 18m x 0 23m (Supersonic)
Stagnation Pressures	40-175 psia (2 7-12x10^5 N/m^2)
Mach No Range	0 2 — 3 5
Reynolds No./m	1 5x 10^7 to 1.0x 10^8
Run Duration	
Maximum	60 secs at Mach 1 0
	35 secs at Mach 3 5
Minimum	10 secs
Storage Tank Volume	85 cum
Storage Pressure (max)	300 psig (2 1 x 10^6 N/m^2
Compressor Motor Power	1 12 x 10^5 W

allows continuous observation of the shock flow in the test-section during the tunnel run.

In order to gain insight of the flow structure ahead and in the vicinity of the obstacle and to measure the separation distances, Surface flow technique was employed to obtain

surface flow patterns for each of the models under investigation. Presently used technique gives a very clear skin friction pattern which is very helpful in understanding the flow structure. The technique employs oil/pigment mixture of vacuum pump oil and Titanium dioxide. The oil/pigment mixture moves in filaments over the surface. Oleic acid is added to this mixture as an additive, dispersing agent, which helps to control the size of the concentrations of the pigment in oil flow. The size of these concentrations in turn determines the proportion and the scale of the streak pattern.

The separation distances were measured from the surface flow pattern obtained after the tunnel run for each of the models. Thereafter, a photograph of each of the flow pattern obtained is taken using a 35mm motorized camera and 135mm focal length lens.

Pressure Model

For the purpose of obtaining streamwise pressure distribution along the axis of symmetry of the plate for each of the models mounted on it, pressure taps of diameter 0.5mm and a pitch of 10mm were drilled along the medial line starting from leading edge of plate. Stainless steel tubes were fixed to the lower side of each of these taps to sense the static pressure on the plate during the interaction process. These

tubes are then taken out through the tunnel floor for pressure measurement into a pressure multiplexing system.

This pressure multiplexing system is a 48-channel multiplexer built around two 24-way cut-off valves which are connected to storage volumes for pressure trappings. The system has a capability of scanning sequentially the storage volumes. The pressure is sensed by a pressure transducer fitted in the stator assembly of the scanivalve. A digital display is provided for readings which consists of pressure port number and pressure in psia and forms a part of the tunnel control console.

The pressure tubes from the plate model are fed into the pneumatic inputs of this pressure multiplexing system. Tunnel run is made for each of the models mounted on the plate. During the run, once the flow is stabilized(which is indicated by a stable running error on the tunnel control console), the scanivalve is brought into action. The scanivalve is brought to "close" mode which traps the air in the multiplexing system. The tunnel run is stopped and the storage volumes with the trapped air are then scanned one at a time by operating the scanivalve in the "Manual" mode. The procedure is repeated for each test model.

Stagnation pressure of each run is also measured using the multiplexer. For this purpose, a stagnation pressure probe is installed in the settling chamber of the tunnel.

Major performance specifications of the pressure multiplexer are listed in Table 2.2 .

Table 2 2

MAJOR SPECIFICATIONS OF PRESSURE MULTIPLEXER

Process Fluid	Air (Clean and Dry)
No of Channels	48
Pressure Range	$0-150$ psia (max.) $[0-1.03 \times 10^6$ $N/m^2]$
Storage Vol /Channel	0 4 cu inch (6 25 cc)
Leakage in Storage Volume	0 006 psi /min (at 10 psi stored press) 55 N/m^2/min (at 0 68$\times 10^5$ stored press)
Pressure Transducer Range	150 psia (1 03 $\times$ 10^6 N/m^2)
Display	(a) Numerical Display of the Pressure Port connected to the transducer (b) Numerical Display of the Pressure in psia.

CHAPTER 3

Results and Discussions

A few of the surface flow patterns typical of those obtained in the investigation are shown as Figs 3.1 to 3.7. Fig 3.2 shows a typical case when the obstacle is at the edge of the boundary layer while Fig 3.4 shows a case where the obstacle height is much larger than the boundary layer thickness. Fig 1.10 sketches the typical flow pattern. Note that in all of them we observe a primary separation line which is indicated by pigment streaks running into it from the two sides. Immediately behind the primary separation line, the flow in front of the obstacle is radially outwards which becomes largely circumferential away from the medial line. One important feature not identified by any earlier observer is a thick pigment line running parallel to the primary separation line. This can be termed as a neck compression shock representing the coming together of the streamlines because of the limited side-flow/pressure relief afforded by the three-dimensional nature of the obstruction.

For obstacles of large heights, one can also very clearly discern a reattachment line very close to the leading edge, and the pattern behind this characterized by the burn-mark on the pigment representing elevated temperatures in the stagnation
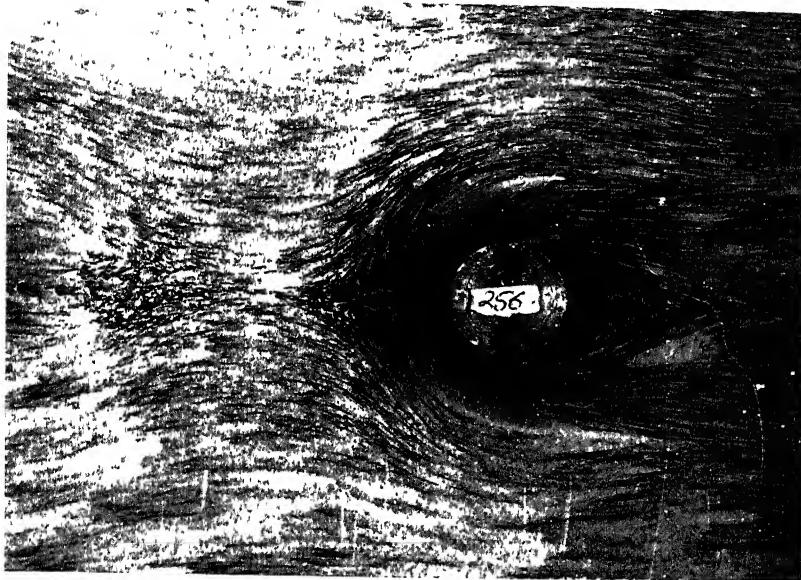
Fig 3.1 Circular cylinder of H=15mm, D=32mm protuding out of
      the boundary layer, δ=3.64mm.
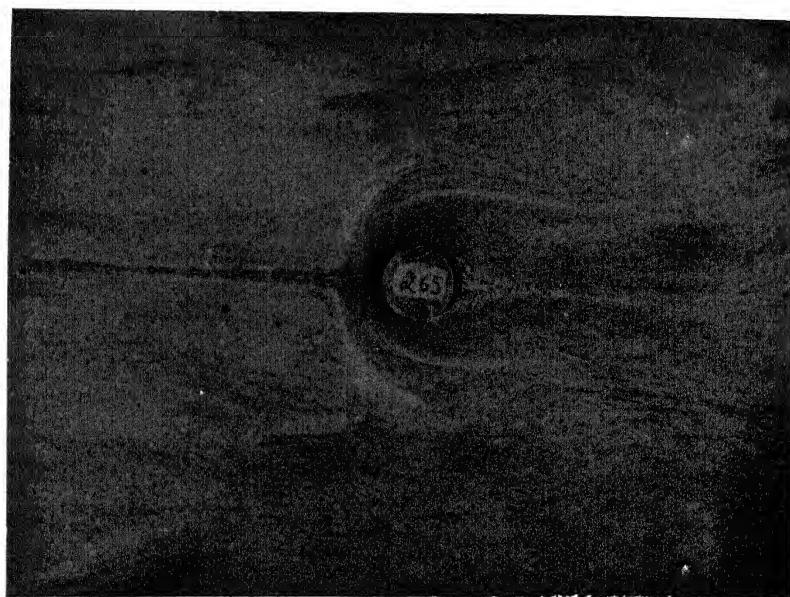

Fig 3.2 Circular cylinder at the edge of the boundary
      layer, H=3mm, δ=2.0mm.
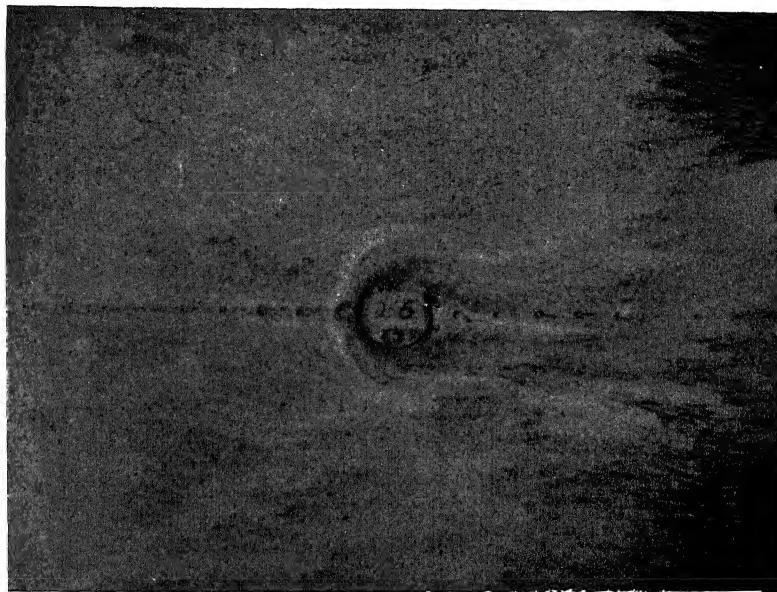
Fig 3.3 Circular cylinder of H=5mm, D=17mm, δ=2.0mm.
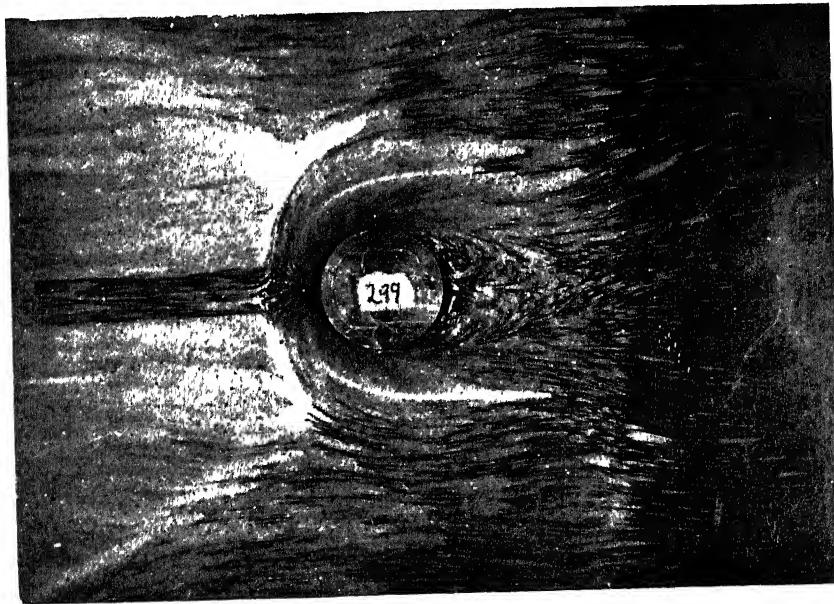
Fig 3.4 Circular cylinder of H=5mm, D=32mm, δ=2.0mm.

Fig 3.5 Circular cylinder of H=15mm, D=32mm, δ=2.0mm.
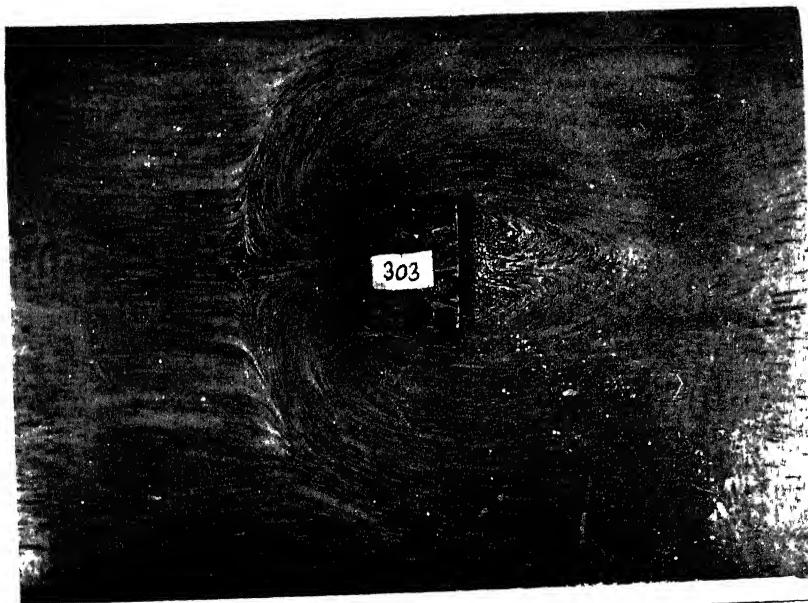
Fig 3.6 Rectangular block of H=10mm, B=32mm, δ=2.0mm.
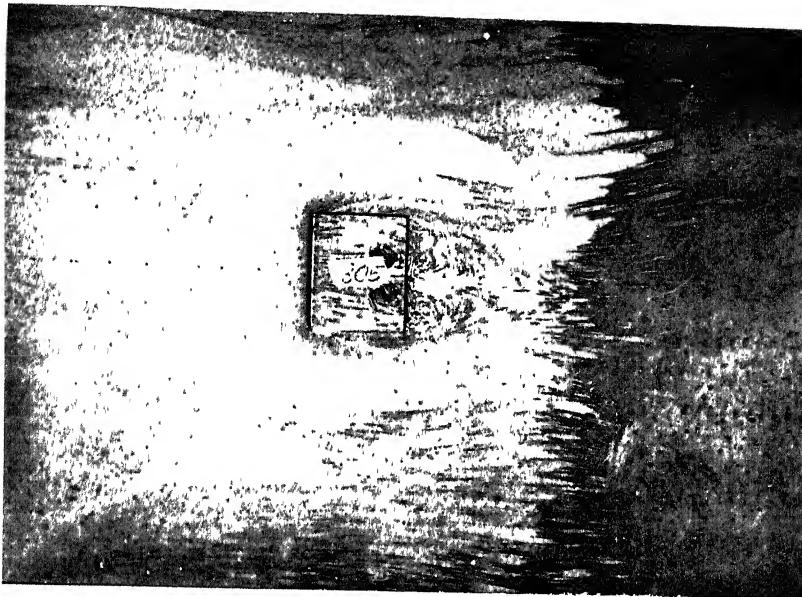
Fig 3.7 Rectangular block of H=3.0mm, B=32mm, δ=2.0mm

flow immediately ahead of the obstacle. The flow pattern thus seen corresponds exactly to the three-layer model proposed by Halprin[6]. This is also confirmed later by the pressure measurements along the medial line.

The flow pattern about the rectangular block are shown in Fig 3.6 & 3.7 and have essentially the same features except that the separation line near the front edges show up. The region in front is essentially a reversed flow region. The circumferential flow develops quite away from the medial line.

In all the flow patterns only one separation line has been observed, quite in line with the observation of Holt[12] who found that for the values of the Reynolds number(based on X, the distance from the leading edge of the splitter plate)

around 10^6, the number of separation lines is only one. Table 3.1 and Table 3.2 give the results of the measurements of separation distance S(along the medial line), ahead of the obstacle and the maximum lateral distance Y of the primary separation line from the edge of the maximum lateral dimension of obstruction for the two flow locations X_1 and X_2 from the leading edge of the plate, resulting in two boundary-layer thicknesses. The data is for various diameters D and height H of the blocks.

A few interesting observations are immediately apparent from the Tables 3.1 and 3.2. At each X location, the primary separation distance S increases with height of the cylinder for same diameter D. The separation distance S appears to have a very little dependence on the diameter of the cylinders. Again, for the cylinders of same height and diameter, the separation distance is more when X is 11cms than when it is 24cms. Since the only parameter changing significantly with X is the boundary layer thickness δ, it increasing with X, it stands to reason that the boundary layer thickness is an important parameter of the flow. Thus one could write

$$S = S(D, H, \delta; M)$$

Various non-dimensionalisations have been attempted in literature. One of the most common one is

Data for circular cylinders mounted at $X_1=24$ cms , $\delta=3.64$ mm

D	H	H/D	H/δ	S	S/D	D/δ	$|Y_{av}|$	$|Y_{av}|/D$	$S/\sqrt{HD}$	$S/\sqrt{\delta D}$
	5	0.156	1.37	1.0	0.313		9.2	0.29	0.8	0.93
32	10	0.313	2.75	17.5	0.55	8.79	18.0	0.56	0.98	1.60
	15	0.469	4.12	23.0	0.72		26.0	0.79	1.05	2.10
	20	0.118	0.55	3.50	0.21		3.50	0.21	0.60	0.44
	25	0.147	0.69	4.40	0.26		4.4	0.26	0.67	0.56
17	30	0.176	0.82	4.70	0.28	4.67	4.7	0.28	0.66	0.60
	50	0.294	1.37	9.0	0.53		8.5	0.50	0.98	1.15
	10	0.588	2.75	12.6	0.741		17.5	1.06	0.97	1.60

TABLE 3.2

Data for circular cylinders mounted at $X_2=11$ cms , $\delta=2.0$ mm

D	H	H/D	H/δ	S	S/D	D/δ	$|Y_{av}|$	$|Y_{av}|/D$	$S/\sqrt{HD}$	$S/\sqrt{\delta D}$
	5	0.156	2.50	1.4	0.44		22.5	0.70	1.11	1.75
32	10	0.313	5.0	22.0	0.69	16.0	41.5	1.29	1.23	2.75
	15	0.469	7.5	27.7	0.87		48.5	1.52	1.26	3.50
	20	0.118	1.0	5.80	0.34		7.30	0.43	0.99	1.0
	25	0.147	1.25	6.30	0.37		9.6	0.56	0.97	1.1
17	30	0.176	1.5	7.0	0.41	8.5	10.0	0.59	0.98	1.20
	50	0.294	2.5	14.0	0.82		24.0	1.41	1.52	2.4
	10	0.588	5.0	18.0	1.06		27.0	1.58	1.38	3.1

All measurements are in mm

$$S/D = f(\ H/D; \ \delta/D; \ M)$$

This has been plotted in Fig 3.8 . A better non-dimensionalisation has been attempted by Sedney, who has plotted

$$S/D = f(\ H/\delta, \ D/\delta; \ M)$$

Fig 3.9 shows such a plot and demonstrates that the separation distance increases for low values of H/δ and then settles down for larger values of H/δ. Infact, most of the increase in S/D occurs for $H/\delta < 1$,i.e. when the obstacle is submerged in the boundary layer.

In analyzing the data, it appears to us that the height H must be non-dimensionalised by δ as done by previous investigators, but the length scale for the separation distance should not be D but some measure of the blockage area that is ultimately responsible in producing the separation. Use of $\sqrt{DH}$ did not lead to any worthwhile results, but $\sqrt{D\delta}$ gave Fig 3.10 wherein all the points for various D, H and δ collapse essentially to one curve.

It is thus clear that the separation distance depends on the length scale of the blockage presented to the boundary layer and on the height of the cylinder with respect to the boundary layer thickness. The diameter of the obstruction has
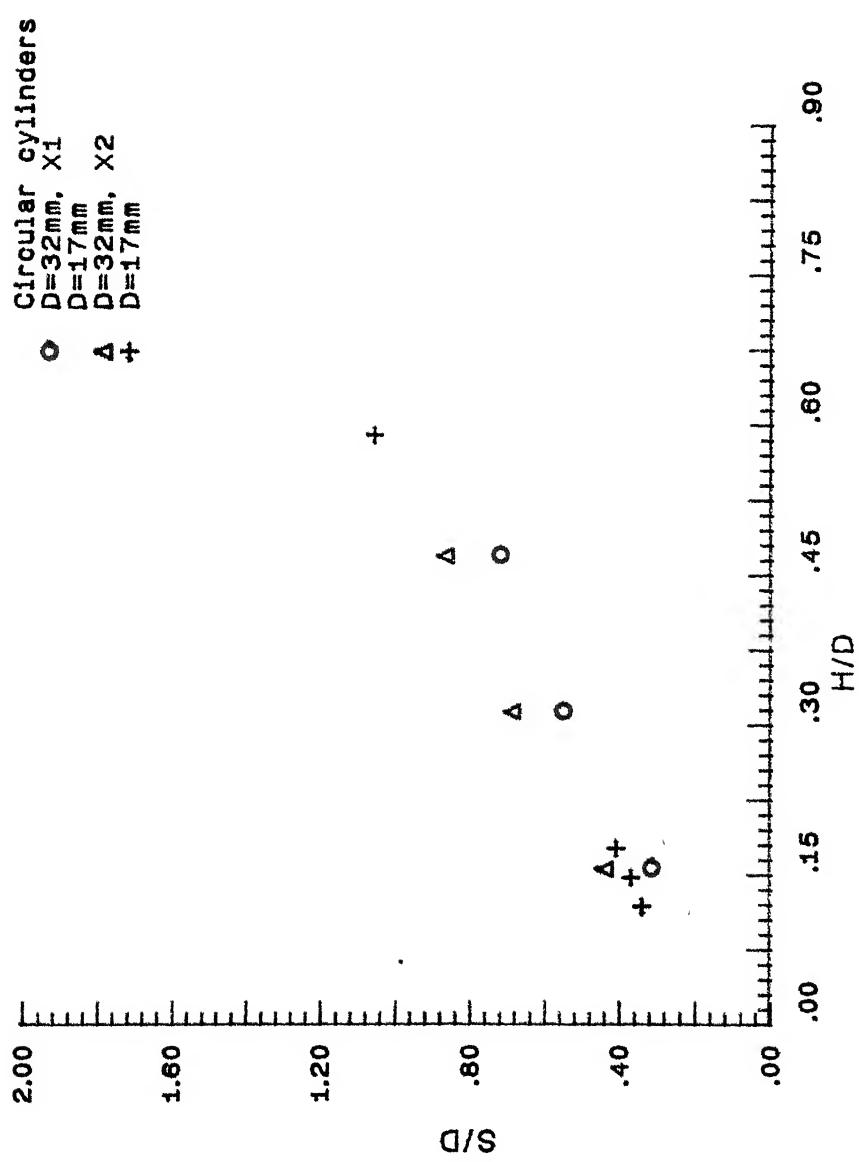
Fig 3.8 Plot showing the effect of height on separation distance
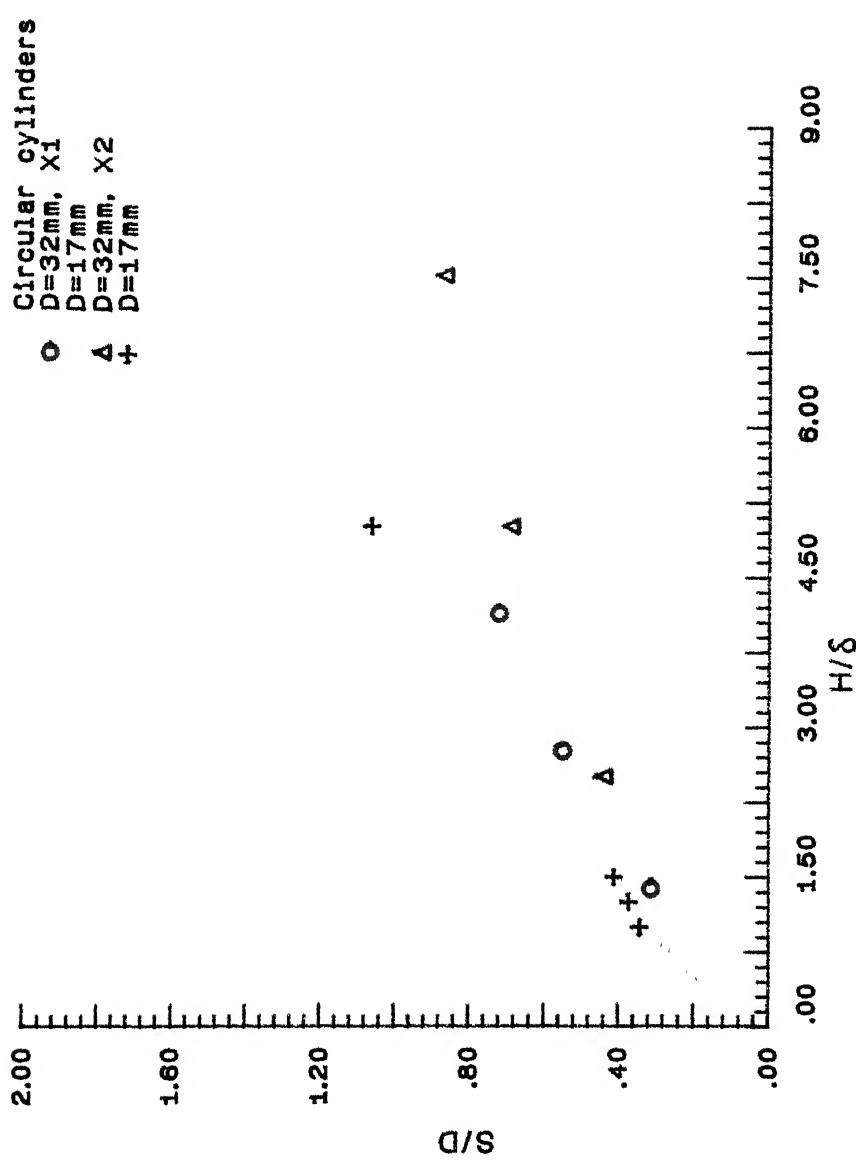
Fig 3.9 Plot showing the effect of height on separation distance
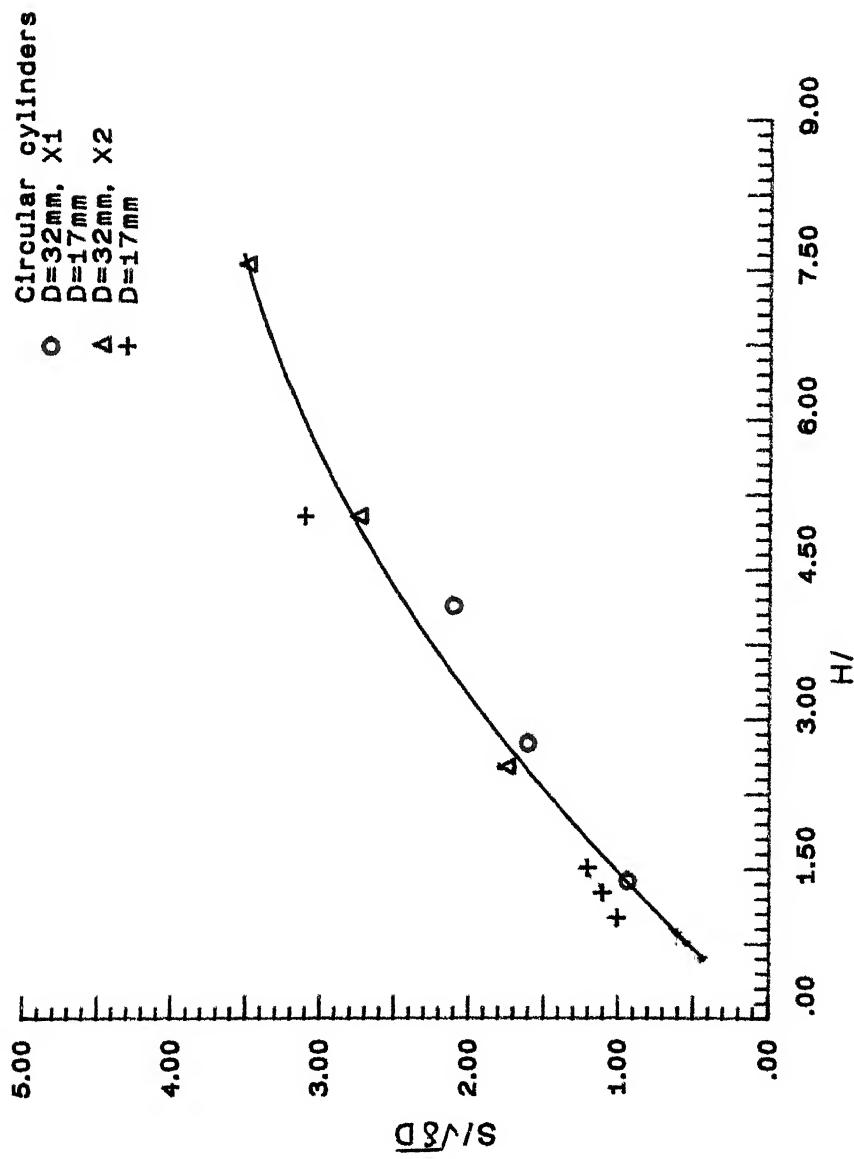
Fig 3.10 Plot showing $S/\sqrt{\delta D}$ vs H/δ

no direct role to play. Thus the standard correlation reported by Westkaemper[7] and used thus far has to be modified. The fact why this effect had so far been missed appears to be the fact that no investigator appears to have taken data at two different boundary-layer thickness locations.

The various points in Fig 3.10 can be correlated by the following relationship

$$S/\sqrt{\delta D} = 0.736(H/\delta) - 0.036(H/\delta)^2$$

The variations in the maximum lateral extent of the separation line are a little more complicated. In general,

$$Y = f(H, D, \delta; M)$$

Since the lateral extent of separation should be a function of the upstream distance S of the separation, this equation was recast by treating S as an independent variable

$$Y/D = f(S/D; M)$$

A plot of this is shown in fig 3.11 which shows that the points for a fixed value of X, the points for different diameters and for different heights all merge into a straight line.
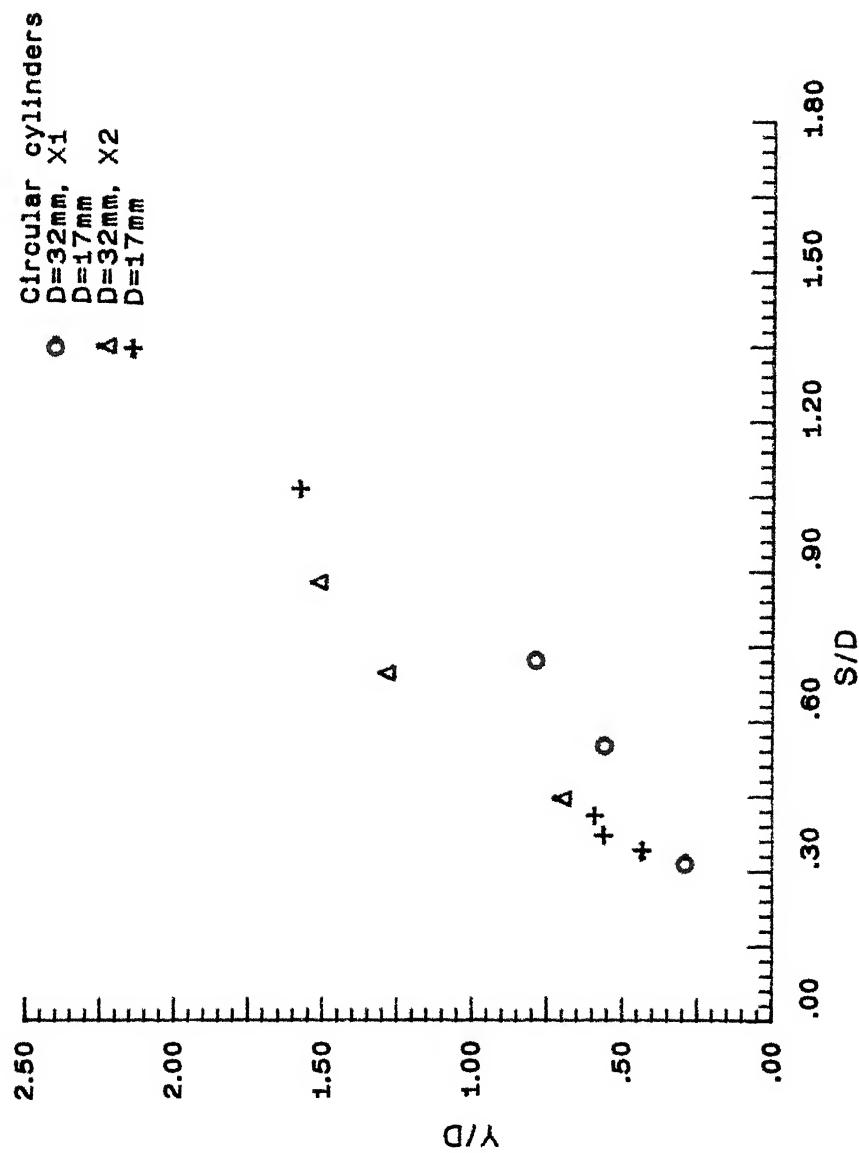
Fig 3.11 Plot showing Y/D vs S/D

Since S is a function of H/δ, non-dimensionalising the independent variable with respect to δ and the dependent variable with respect to D, we obtain

$$Y/D = f(H/\delta, D/\delta; M)$$

Fig 3.12 shows the plot of this and it is noticed that the dependence of D/δ is rather small so that we can develop an approximate correlation as,

$$Y/D = 0.356(H/\delta) - 0.02(H/\delta)^2$$

Some other non-dimensionalising were also attempted. Fig 3.11 shows a plot of Y/D vs S/D where the separation distance is used as an independent variable. It is noticed that the individual points do fall along straight lines but the dependence on X and hence δ cannot be ignored.

Fig 3.13 shows a plot of Y/D vs $S/\sqrt{\delta D}$ to take care of X dependence. The plot does appear to give a satisfactory reduction but the choice of S as an independent variable is not very satisfactory.

We have been unable to find any data in literature for rectangular blocks. Here we have attempted to study the effects of change in protuberance geometry. Some similar observations
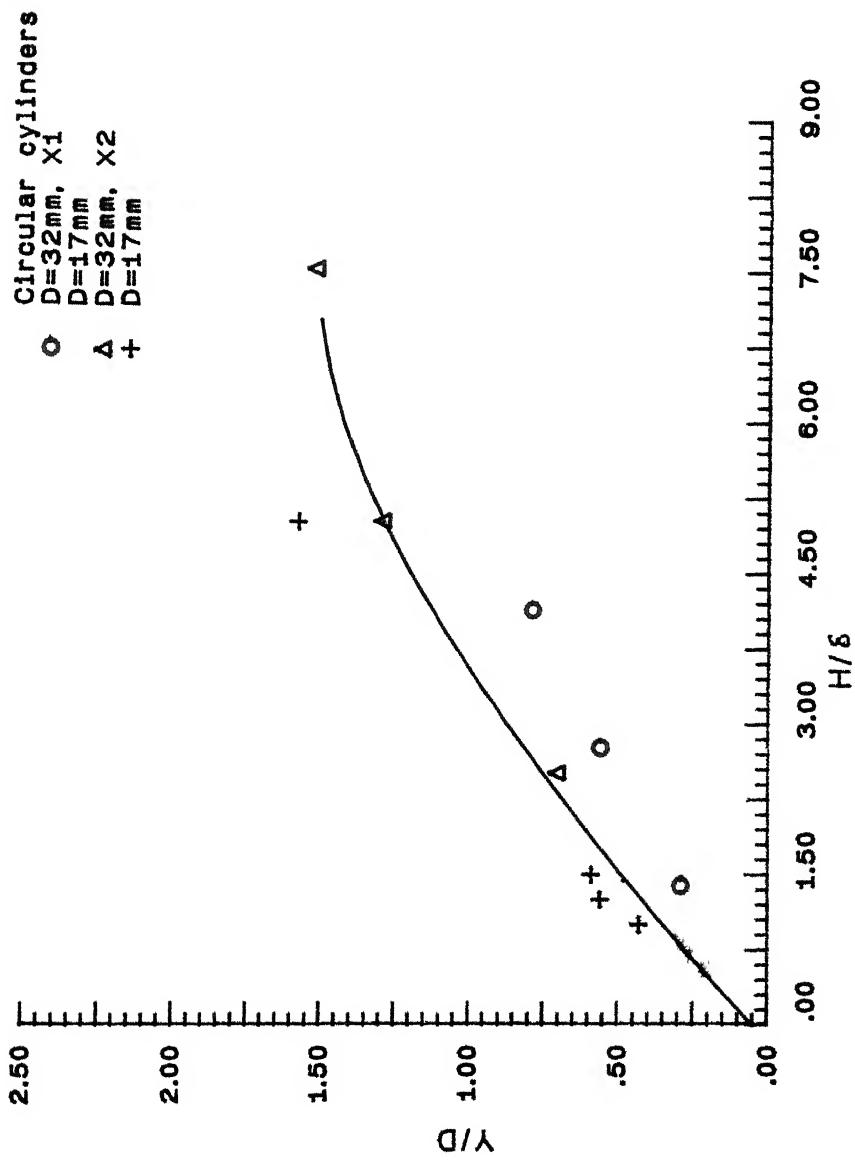
Fig 3.12 Plot showing Y/D vs H/δ
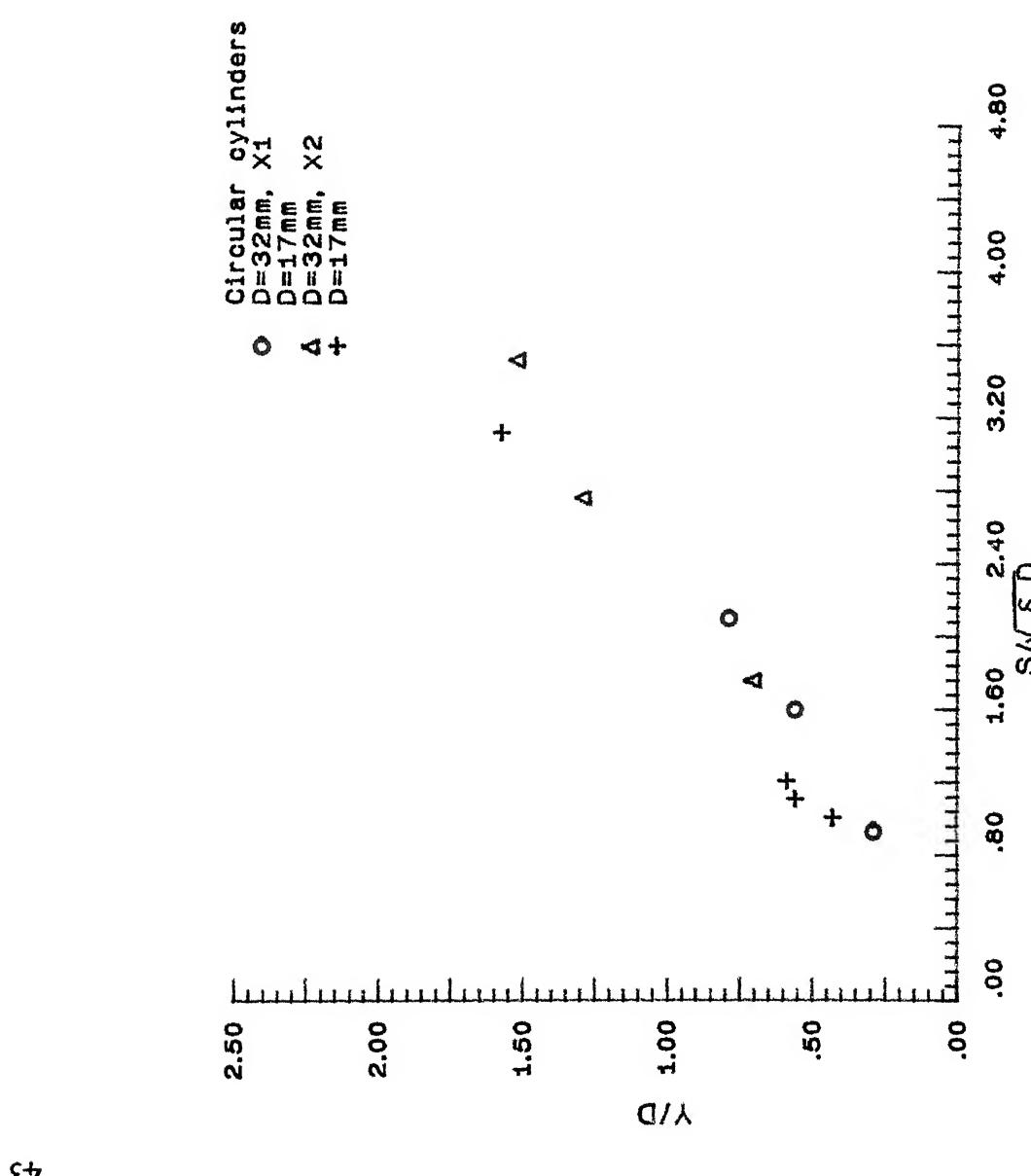
Fig 3.13 Plot showing Y/D vs S/√δD

Circular cylinders
o   D=32mm, X1
    D=17mm
Δ   D=32mm, X2
+   D=17mm

S/√δD

Y/D

have been made for rectangular blocks as well. Here B is used to represent the lateral dimension of the rectangular block. Table 3.3 and Table3.4 show the data obtained from tests for various heights of blocks mounted at X_1 and X_2 locations respectively.

Some interesting features are observed when the data for this case is compared with that of circular cylinders. For rectangular blocks, it is seen that the separation distance S is greater when compared with a similar case of circular cylinder. separation distance S shows a dependence on height H of the block for a particular X location. However, for same height of the block, S is greater for X_2 location than for X_1 location.

On the basis of similar explanation as given for circular cylinders, separation data is plotted for rectangular blocks.

Fig 3.14 shows the plot for S/B vs H/δ where it is observed that the separation distance increases for low values of H/δ and tends to settle down for larger values H/δ.

Fig 3.15 shows a plot for $S/\sqrt{\delta B}$ vs H/δ. The points follow a curve for which we can develop a correlation as,

$$S/\sqrt{\delta B} = 1.017(H/\delta) - 0.05(H/\delta)^2$$

TABLE 33

Data for rectangular blocks mounted at $X_2=24$ cms , $\delta=3.64$ mm

B	H	H/B	H/δ	S	S/B	B/δ	$|Y_{av}|$	$|Y_{av}|/B$	$S/\sqrt{\delta B}$
	3	0.094	0.82	5	0.156		4.9	0.15	0.46
	5	0.156	1.37	12.7	0.397		14.0	0.44	1.18
32	10	0.313	2.75	36.0	1.13	8.79	37.0	1.16	3.33
	15	0.469	4.12	54.0	1.69		56.0	1.75	5.0

TABLE 34

Data for rectangular blocks mounted at $X_2=11$ cms , $\delta=2.0$ mm

B	H	H/B	H/δ	S	S/B	B/δ	$|Y_{av}|$	$|Y_{av}|/B$	$S/\sqrt{\delta B}$
	3	0.094	1.5	12.2	0.38		14.4	0.45	1.53
	5	0.156	2.5	18.9	0.59		25.3	0.79	2.36
32	10	0.313	5.0	29.3	0.92	16.0	41.0	1.28	3.66
	15	0.469	7.5	39.2	1.23		50.0	1.56	4.9

All measurements are in mm
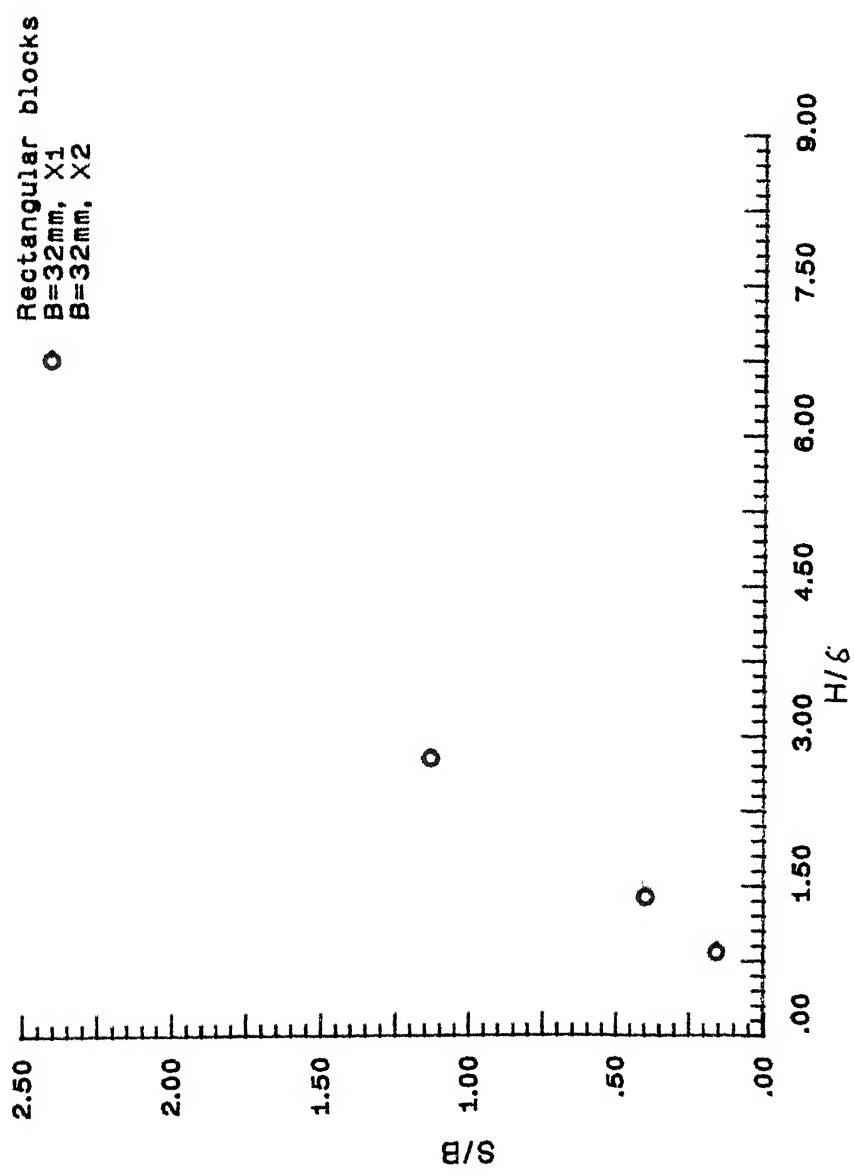
Fig 3.14 Plot showing S/B vs H/δ

Legend:
- Rectangular blocks
- B=32mm, X1
- B=32mm, X2

Axes:
- S/B (vertical): 2.50, 2.00, 1.50, 1.00, .50, .00
- H/δ (horizontal): .00, 1.50, 3.00, 4.50, 6.00, 7.50, 9.00

Fig 3.15 Plot showing S/√δB vs H/δ

* sbv * cc-11t/k : vayu * 05/05/93 15: 31: 34 *
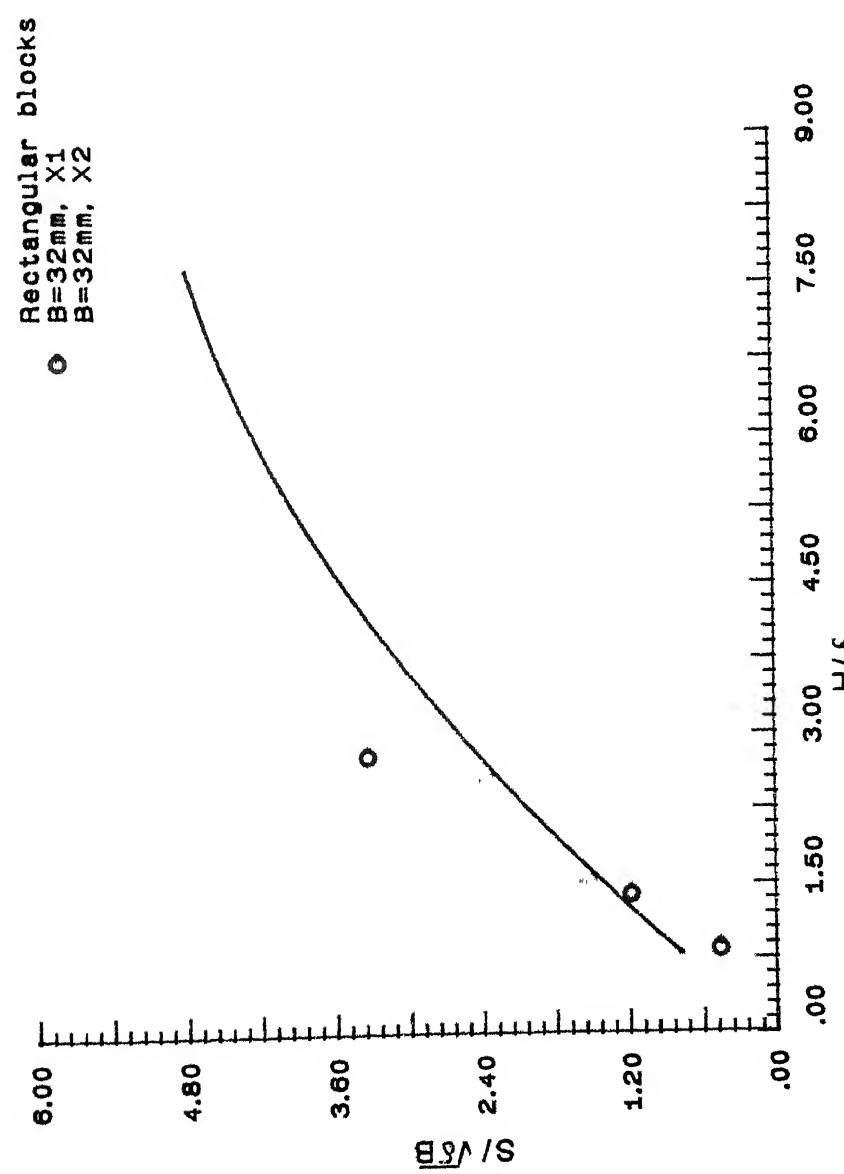
In a similar way, the maximum lateral extent of the separation line is studied as a function of the upstream distance S of separation for rectangular blocks.

A plot of Y/B vs S/B is shown in Fig 3.16. It is observed that for fixed X location, the points for various heights of blocks merge into a straight line.

Fig 3.17 shows a plot for Y/B vs H/δ wherein it is noticed that the points for X_1 and X_2 locations merge into a curve. As a result an approximate correlation was developed given by,

$$Y/B = 1.7 - 2.06 \ e^{-0.342(H/δ)}$$

Fig 3.18 shows a plot for Y/B vs S/$\sqrt{δB}$ to take care of X dependence. It is seen that the points fall into a straight line.

The variation of pressure along the medial line is shown in Figs 3.20 to 3.25 . These pressure plots follow the same pattern as expected from the work of Ozcan and Holt[12] . The pressure begins to rise further upstream as the height of the obstruction increases. But whereas for the cylinders with lower values of H/δ, the pressure keeps rising as we approach the obstruction, in the case of large values of H/δ the pressure peak does not occur at the obstruction plate junction, but rather a small distance out along the plate.

The pressure rises again towards the plate obstruction-
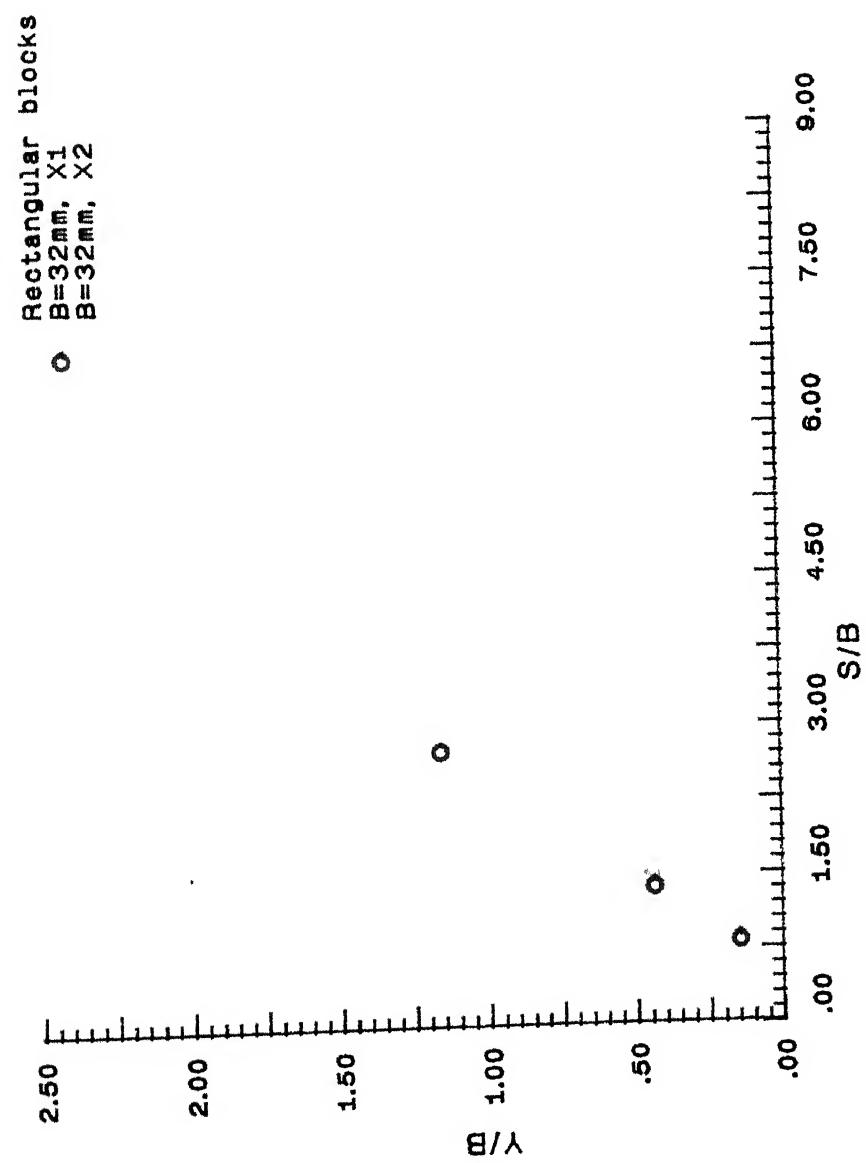
Fig 3.16 Plot showing Y/B vs S/B
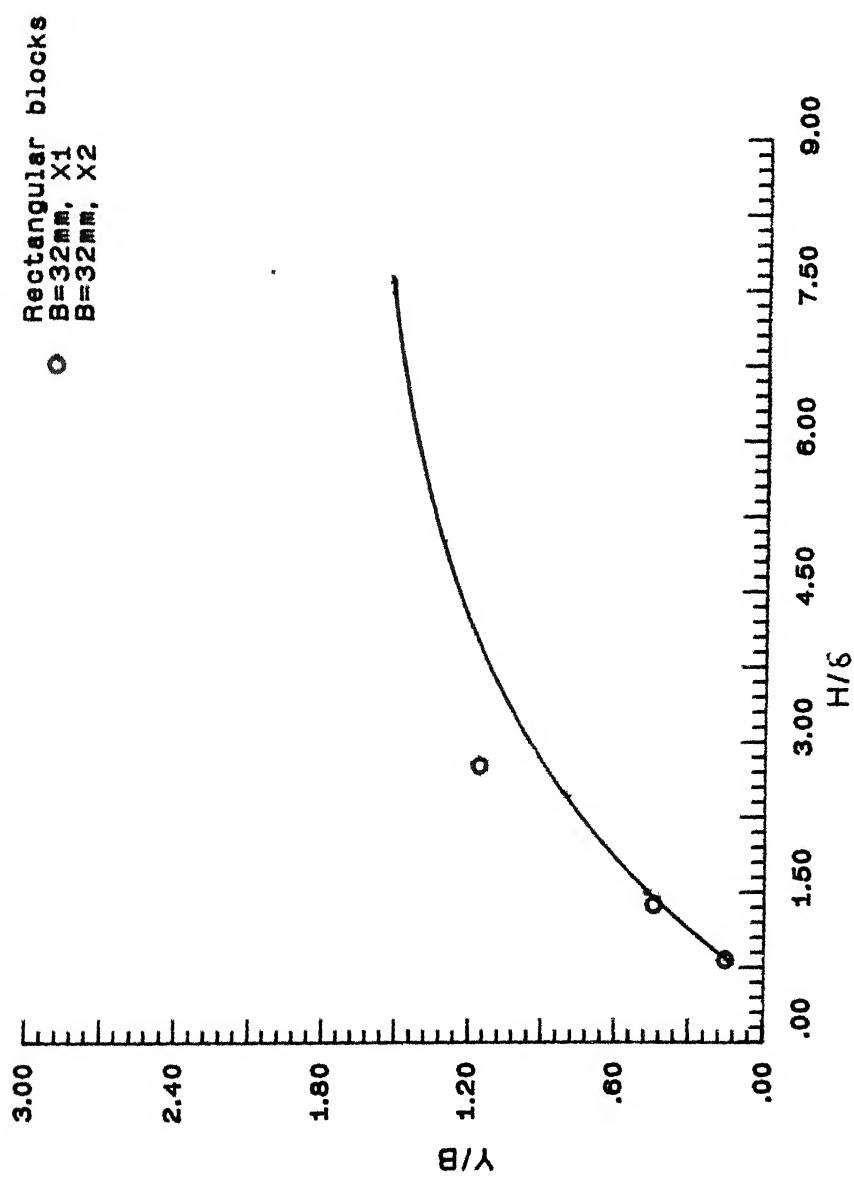
Fig 3.17 Plot showing Y/B vs H/δ

* sbv * cc-iit/k ; vayu * 05/05/93 17:26:33 *
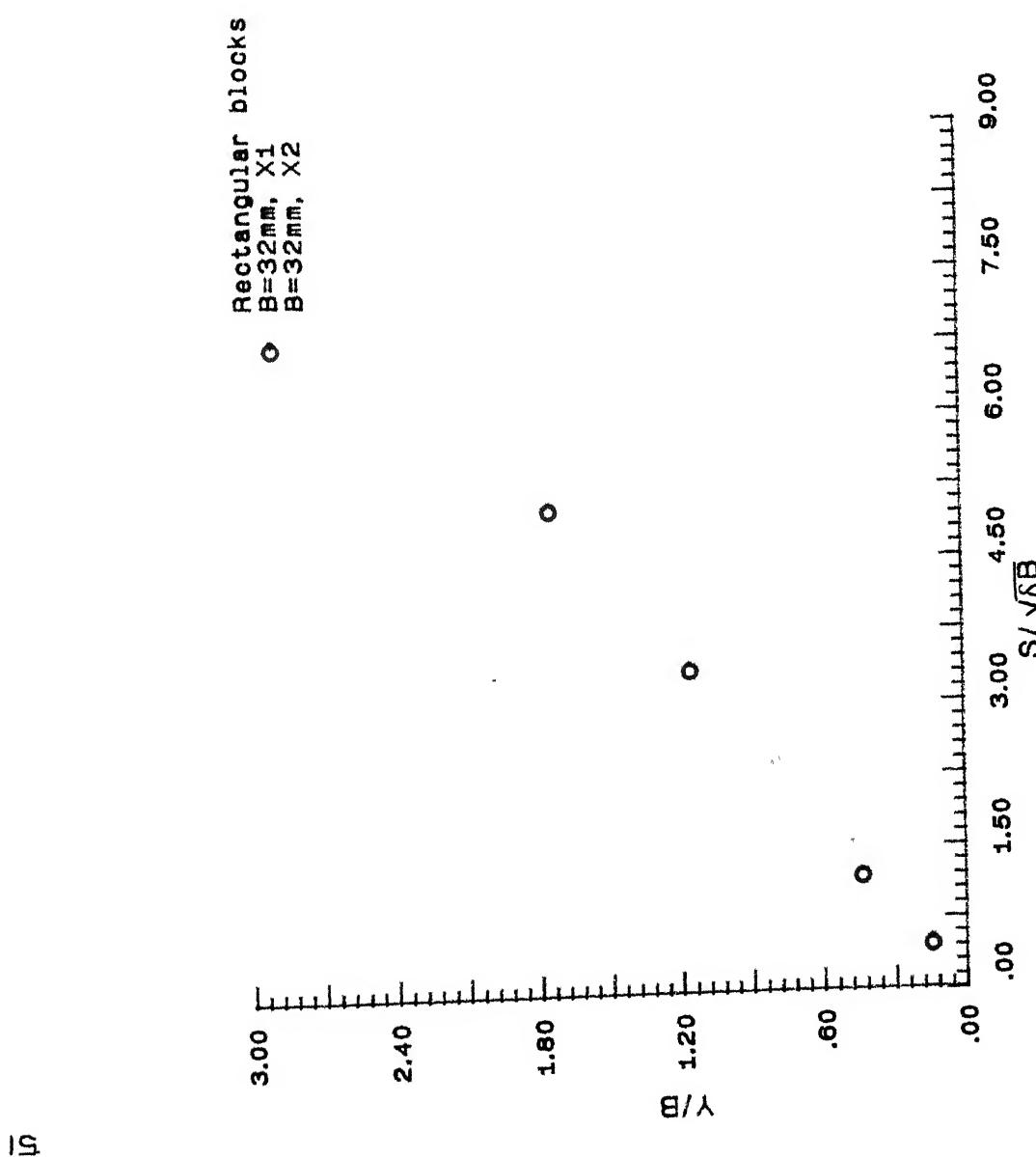
Fig 3.18 Plot showing Y/B vs S/√δB

Rectangular blocks
o B=32mm, X1
   B=32mm, X2

S/√δB

Y/B

3.00 2.40 1.80 1.20 .60 .00

.00 1.50 3.00 4.50 6.00 7.50 9.00
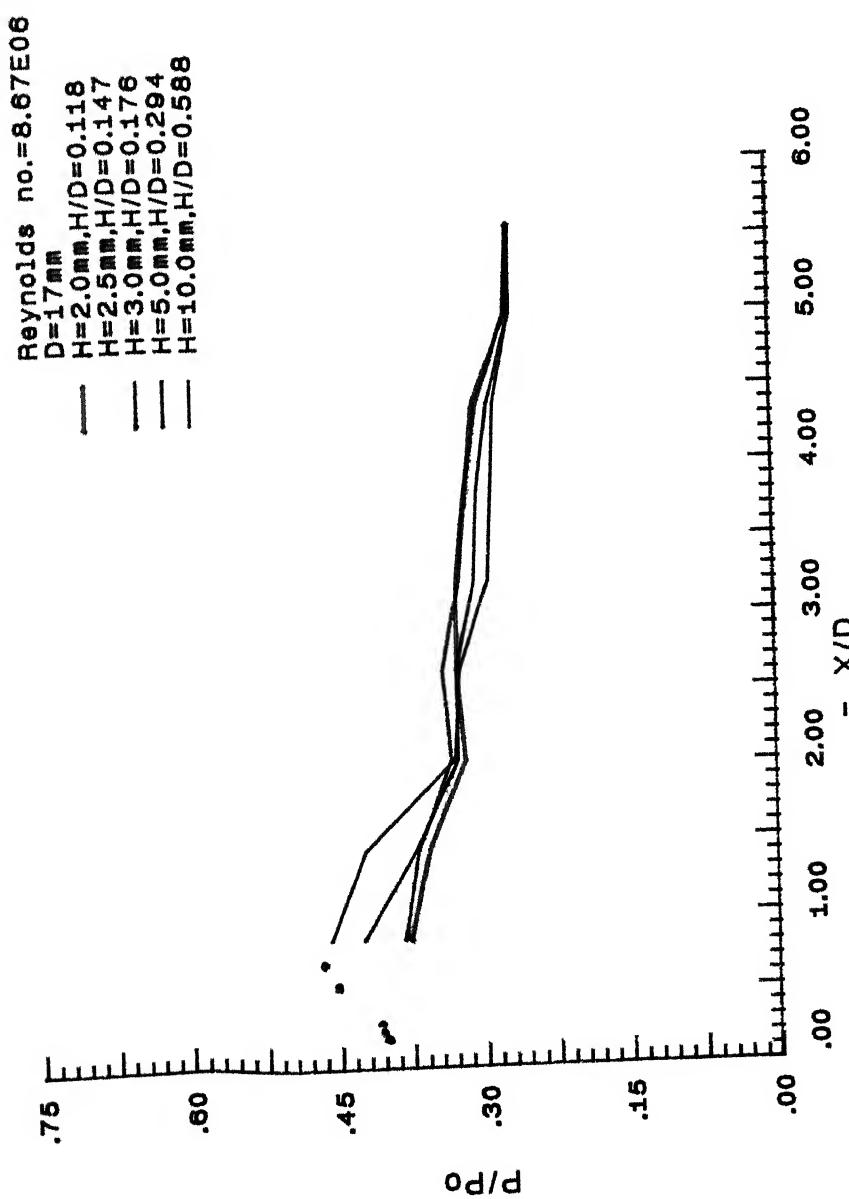
Fig 3.20 Streamwise pressure distributions for circular
cylinders at X1=24cms,Y=0,M=1.6
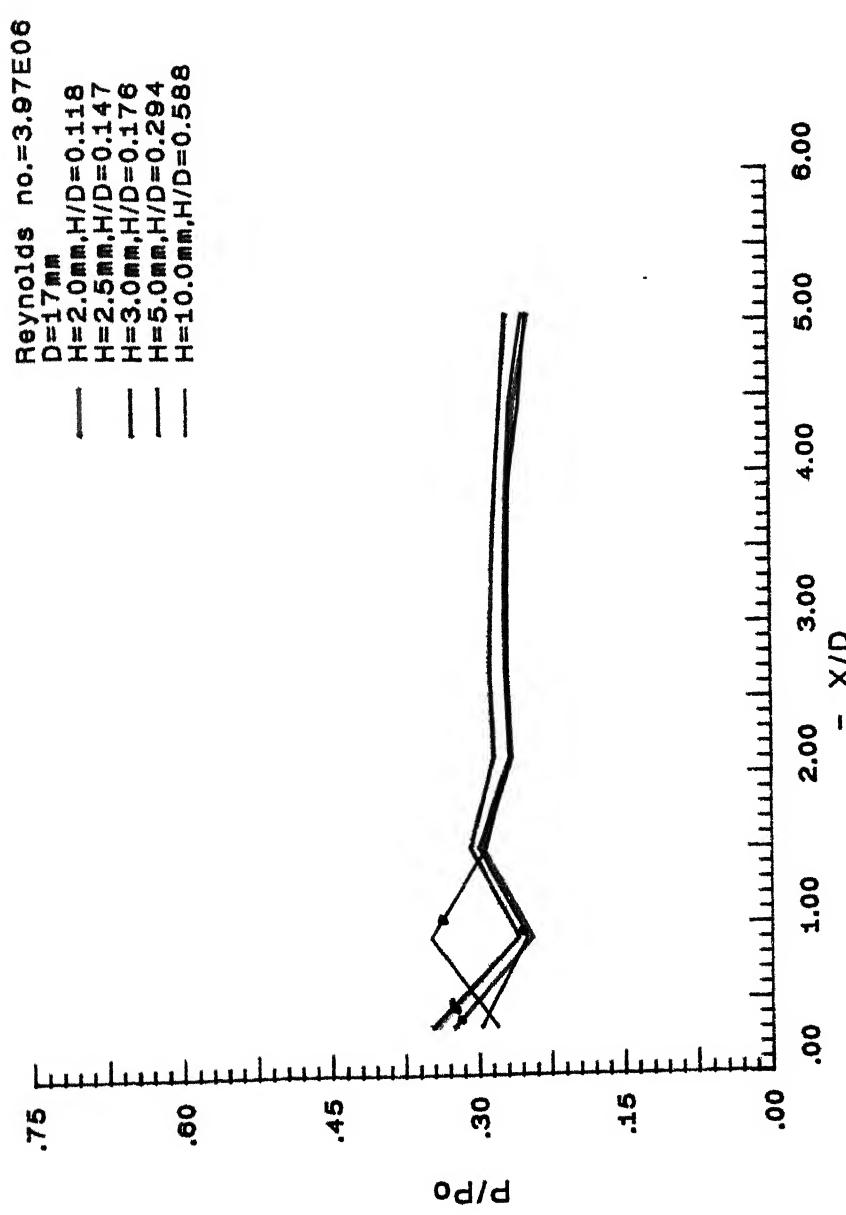
Fig 3.21 Streamwise pressure distributions for circular
cylinders at X2=11cms,Y=0,M=1.6
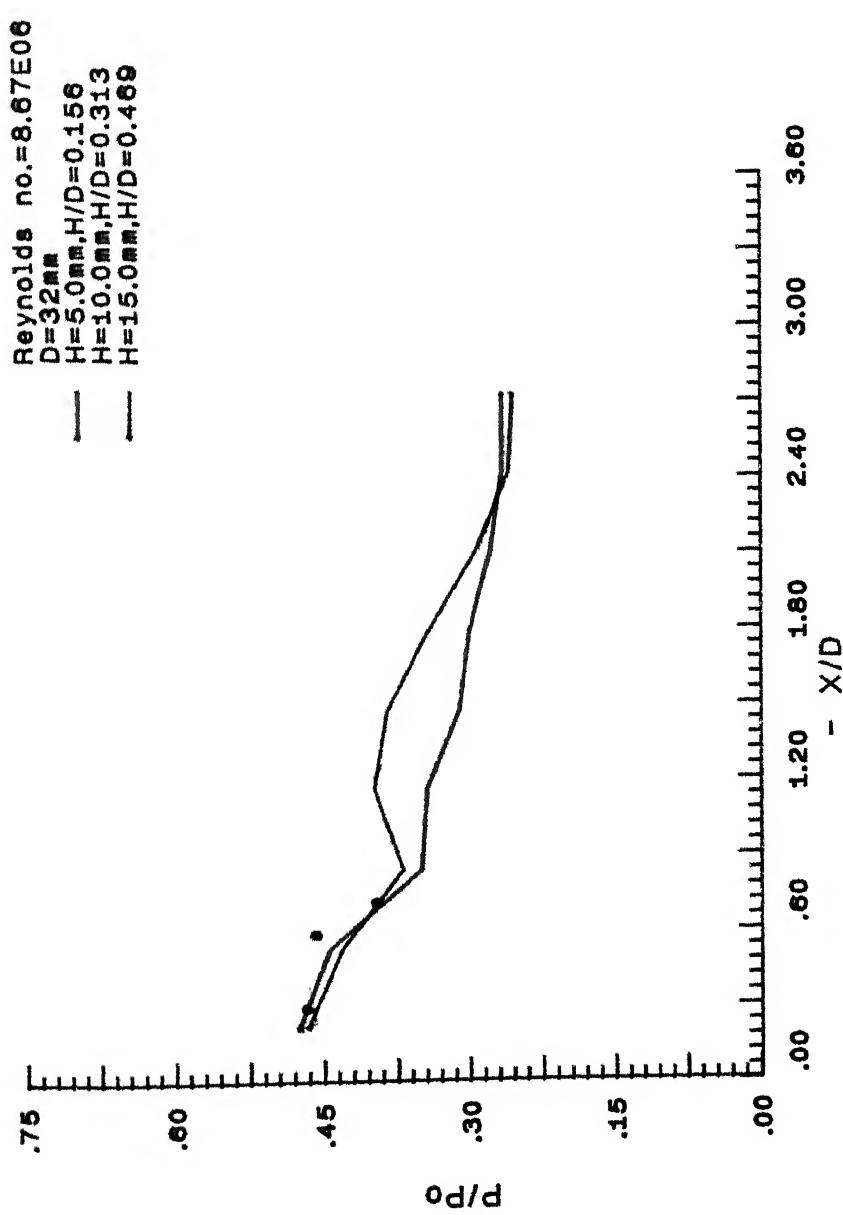
Fig 3.22 Streamwise pressure distributions for circular
          cylinders at X1=24cms,Y=0,M=1.6
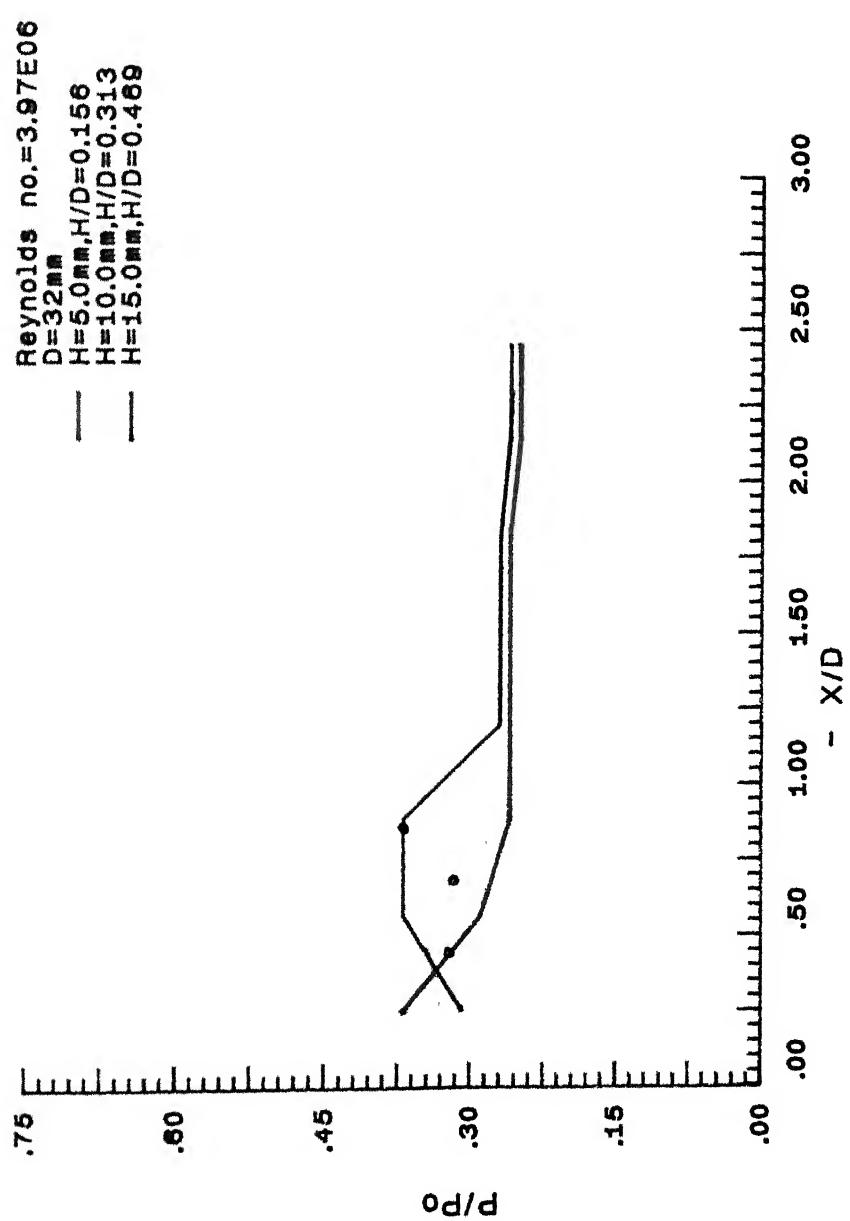
Fig 3.23 Streamwise pressure distributions for circular
cylinders at X2=11cms,Y=0,M=1.6
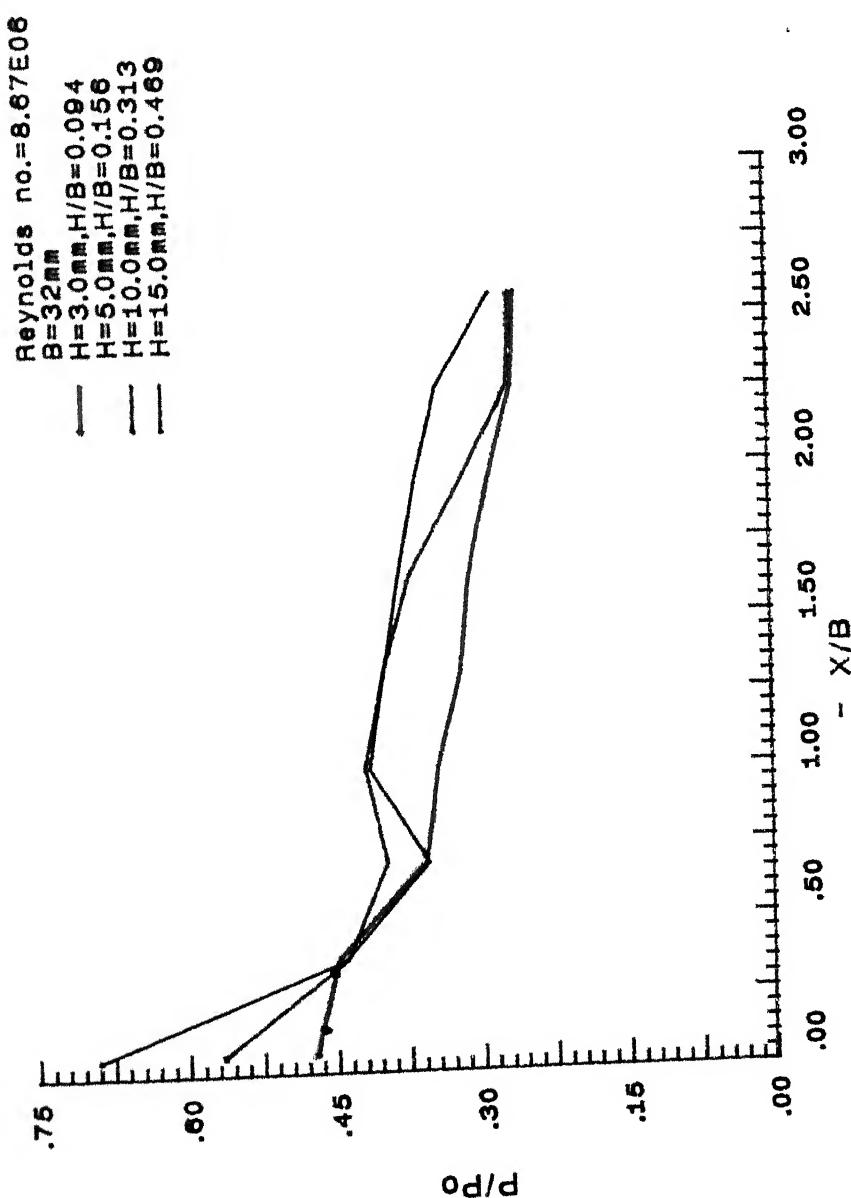
Fig 3.24   Streamwise pressure distributions for rectangular steps at X1=24cms,Y=0,M=1.6

Reynolds no.=8.67E06
B=32mm
H=3.0mm,H/B=0.094
H=5.0mm,H/B=0.156
H=10.0mm,H/B=0.313
H=15.0mm,H/B=0.469

P/Po

- X/B

Fig 3.25 Streamwise pressure distributions for
rectangular steps at X2=11cms,Y=0,M=1.6

Reynolds no.=3.97E06
B=32mm
——— H=3.0mm,H/B=0.094
——— H=5.0mm,H/B=0.156
——— H=10.0mm,H/B=0.313
——— H=15.0mm,H/B=0.469

* sbv * cc-iit/k : vayu * 05/06/93 05: 33: 17 *
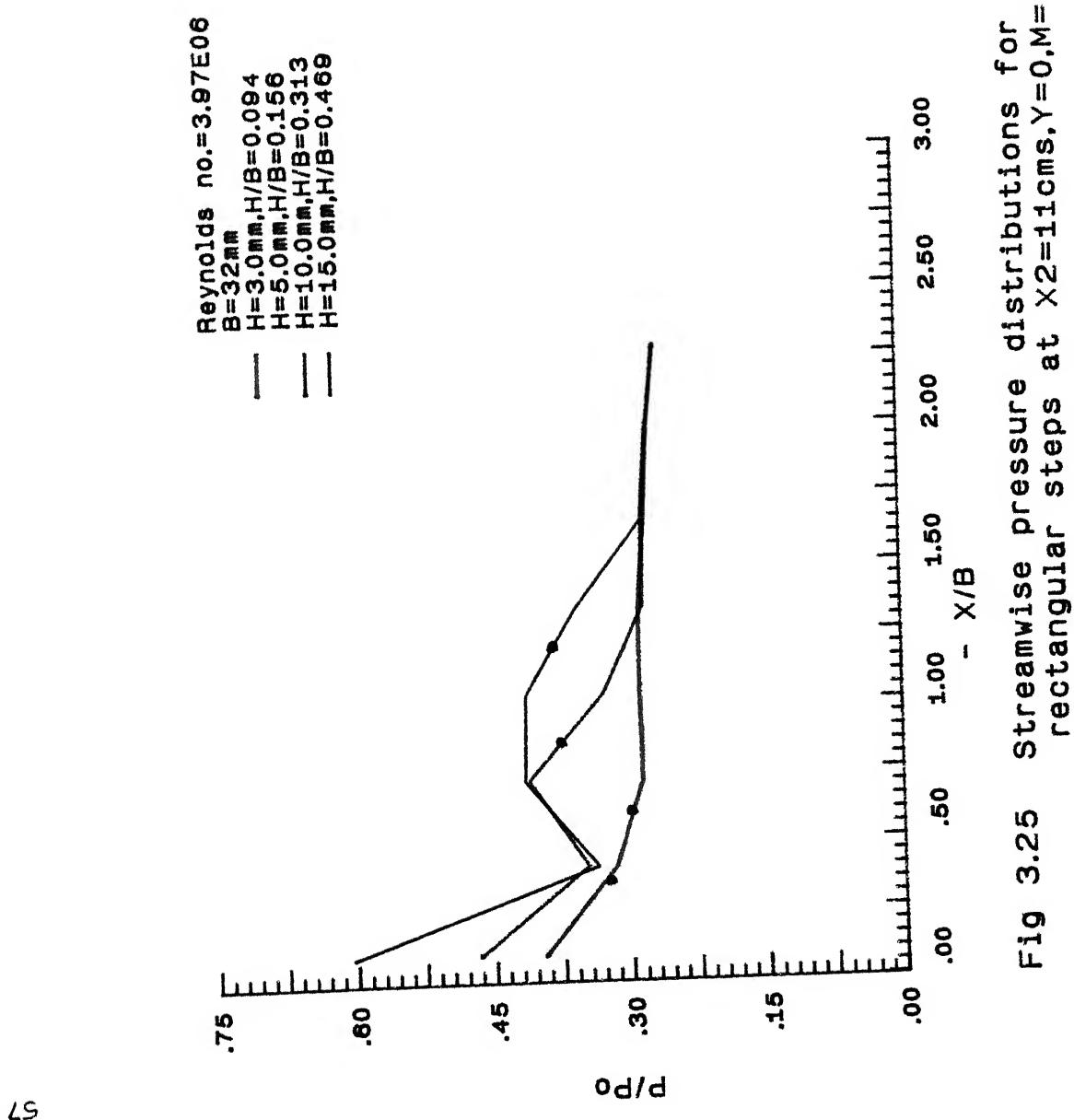
junction, suggesting as before that reattachment of flow has occurred and that the flow is proceeding towards a stagnation point.

But this is as far as the agreement of the pressure profiles with those obtained by Ozcan and Holt goes. There results are shown in Fig 3.25 show a similar P/P_o versus X/D profile for various values of H, D and H/D. We notice no such thing in our case. Cylinders of larger height start showing a pressure rise at much larger values of X/D ahead of the cylinder than for smaller heights.

Another feature worth observing is that for greater H values, a greater pressure drop after the first rise is experienced, after which the pressure rises to a greater peak pressure near the plate-obstruction junction. However the unavailability of a pressure hole near the plate-obstruction junction for some cases, the plots do not reveal the final pattern discussed. Such cases show a pressure drop pattern at some distance out along the plate.

As experienced by earlier observers, it was found difficult to predict the separation distance from pressure plots. So for our convenience we have marked the separation distances on the pressure plots for each case under investigation. For most of the cases it is observed that the separation results between the first pressure rise from the undisturbed value and the significant pressure drop. However, for cylinders with small
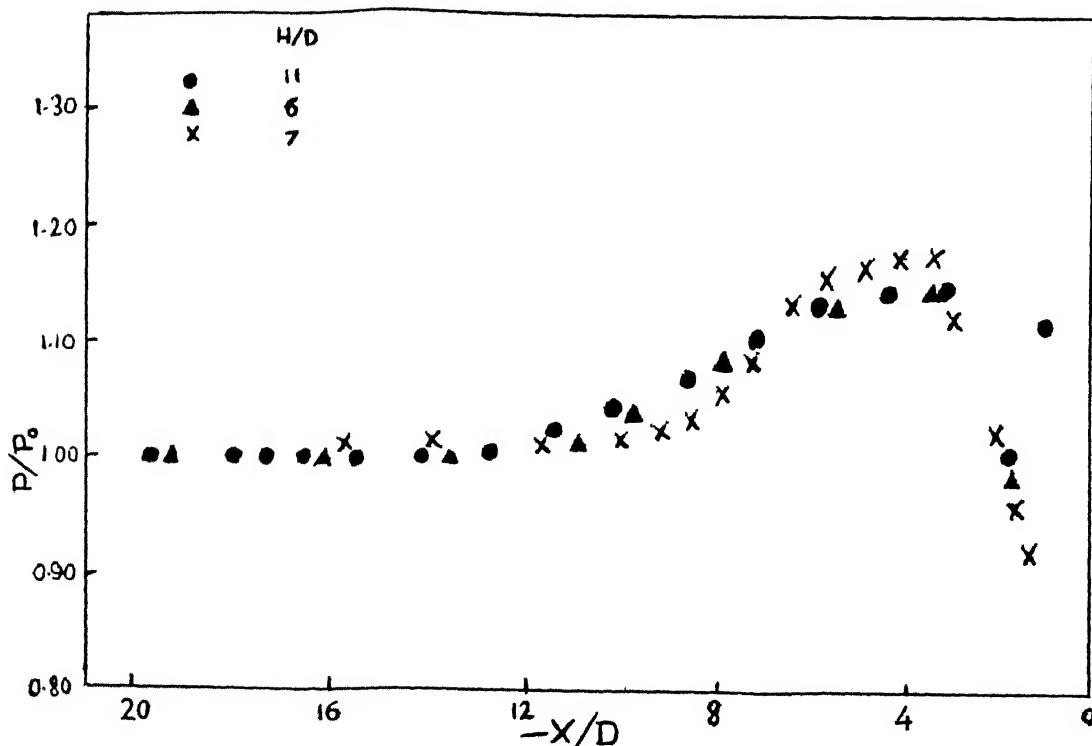
Fig 3.26 Streamwise pressure distributions as obtained by
Ozcan and Holt

heights and D=17mm, no particular trend could be found because
of the small separation distances that were obtained which as a
result extend out of the plots.

An attempt of reduction of the curves by scaling the x
distance with S instead of with D also failed as seen in Fig
3.27 to 3.28.

It may be noticed that the spacing between the pressure
taps is rather large in our experiments. This does not permit
high resolution. The repeatability of the pressure profiles is
quite good with variations in P/P_0 being less than 0.02 .
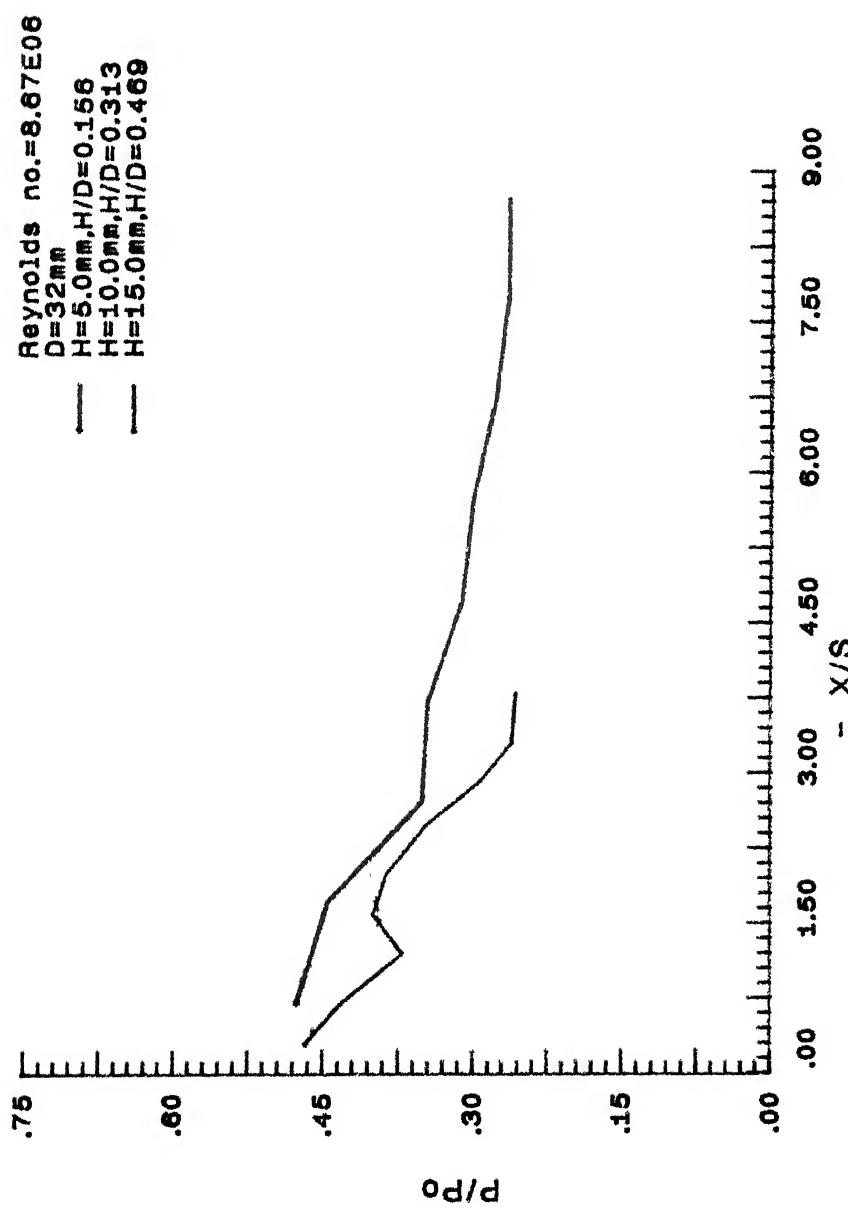
Fig 3.26 Streamwise pressure distributions for circular
cylinders at X1=24cms,Y=0,M=1.6

Reynolds no.=8.67E06
D=32mm
H=5.0mm,H/D=0.156
H=10.0mm,H/D=0.313
H=15.0mm,H/D=0.469

P/Po

- X/S
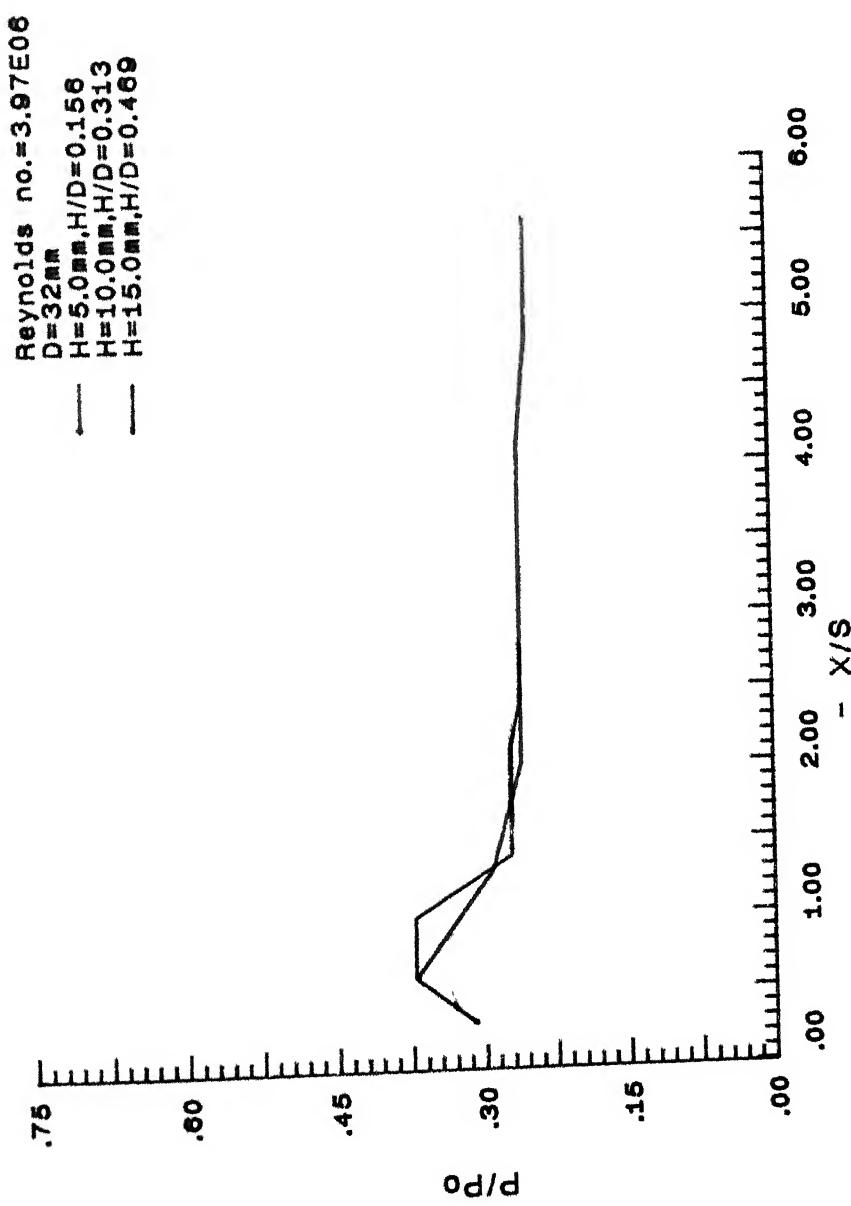
Fig 3.27 Streamwise pressure distributions for circular
cylinders at X2=11cms,Y=0,M=1.6

Conclusions

(i)   The separation distance S depends very strongly on the boundary-layer thickness δ.

(ii) For the cylinder of same height and diameter, separation distance decreases with δ.

(iii) The appropriate length scale for H is δ and that for S is a length based on the boundary-layer blockage area. Thus, $S/\sqrt{\delta D}$ when plotted against H/δ, all points collapse quite well on to a single curve which can be correlated as

$$S/\sqrt{\delta D} = 0.736(H/\delta) - 0.036(H/\delta)^2$$

(iv) The maximum lateral extent of the primary separation line Y/D when plotted against H/δ, it is observed that the points merge into a curve for which a correlation has been developed as

$$Y/D = 0.356(H/\delta) - 0.02(H/\delta)^2$$

(v)   Correlations have also been developed for rectangular blocks for the plots $S/\sqrt{\delta B}$ vs H/δ and Y/B vs H/δ where the points follow a curve governed by the relations

$$S/\sqrt{\delta B} = 1.017(H/\delta) - 0.0513(H/\delta)^2$$

and $Y/B = 1.7 - 2.06\ e^{-0.342(H/\delta)}$

respectively.

(vi) Westkaemper's correlation could not be used for our case due to it's limit to only large obstacles.

Turbulent Boundary Layer at Moderate to High Reynolds Number," **AIAA Journal**, Vol. 14, Jan. 1976, pp. 50-56.

14. Van Driest, E.R.,"Turbulent Boundary layer in Compressible Fluids", **Journal of Aeronautical Sciences**, Vol. 18, No. 3, March 1951, pp. 145.